Sensitivity assessment of bathymetry and choice of tidal constituents on tidal stream energy resource characterisation in the Gulf of California, Mexico

Mejia-Olivares, Carlos; Haigh, I.D.; Lewis, Matthew; Neill, Simon

Applied Ocean Research

Peer reviewed version

Cyswllt i'r cyhoeddiad / Link to publication

1 # Sensitivity assessment of bathymetry and choice of
2 # tidal constituents on tidal-stream energy resource
3 # characterisation in the Gulf of California, Mexico.

4

5 **Carlos Joel Mejia-Olivares[1], Ivan D. Haigh[1], Matt J. Lewis[2] and Simon P. Neill[2]**

6 [1] School of Ocean and Earth Science, National Oceanography Centre, University of Southampton, European

7 Way, Southampton, SO14 3ZH, U.K.

8 [2]School of Ocean Sciences, Bangor University, LL59 5AB, UK.

9

10

11

12

13

14

15

16

17 **Corresponding author**
18 E-mail address: carlos.mejia-olivares@noc.soton.ac.uk (Carlos Joel Mejia-Olivares).
19 Ocean and Earth Science, National Oceanography Centre, University of Southampton,
20 European Way, Southampton, SO14 3ZH, U.K.

21

22

23

24

27

28

29

30

31

32

33

34

Abstract

There has been a significant increase in the number of published tidal-stream energy resource assessments in recent years due to the growing availability of open-source hydrodynamic models, and freely available data for model bathymetry (e.g. GEBCO_2014 and ETOPO) and boundary conditions (e.g. TPXO, FES, EOT). This study examines how the choice of bathymetry and tidal constituents affects the quantification of a tidal-stream energy resource, by conducting sensitivity tests for the Gulf of California. We find that the mean KPD (Kinetic Power Density) and annual mean power are significantly underestimated when using just GEBCO_2014 or ETOPO bathymetry data sources on their own. For the Midriff region, between San Lorenzo and San Esteban Islands (herein the San Lorenzo Passage), the annual mean power potential was estimated to be around 50 MW when using freely available bathymetry data, while the annual mean power increased to ~200 MW when using a bespoke dataset that was a combination of GEBCO and higher-resolution bathymetry provided by CICESE (The Centre for Scientific Research and Higher Education at Ensenada). Current speeds reduce from 2.4 m/s when using high-resolution to around 1.2 m/s and 0.8 m/s when using open source bathymetry products. Finally, we compared the estimated energy using tidal levels predicted from 29 tidal constituents compared with simulations that included just the principal semi-diurnal lunar (M_2) and solar (S_2) constituents. The annual mean KPD reduced by almost $1/3^{rd}$ in the San Lorenzo Passage, when just considering M_2 and S_2 constituents, suggesting that diurnal and higher order harmonic constituents are important for accurate resource assessments in this region.

Key words: Tidal-stream energy, bathymetry, sensitivity tests, annual mean power, GEBCO, ETOPO, Gulf of California, Mexico

1. Introduction

Over the last two decades, there has been increased interest in tidal energy exploitation [1]. Tidal energy offers many benefits compared to other sources of renewable energy, because of the regular and predictable nature of tides [2]. There are two main ways of harnessing tidal energy: (1) tidal range via the use of tidal barrages or lagoons; and (2) tidal current (tidal-stream). Tidal barrages or lagoons are major constructions that are generally associated with relatively high environmental impacts [3]. In contrast, tidal-stream generators make use of the kinetic energy of moving water to power turbines [2], similar in principle to wind turbines. The main differences are the flow density and the thrust that each device is capable of tolerating under regular operational conditions. The kinetic energy in Marine current devices is defined as the movement of the total velocity of the current across the swept area of a horizontal axis device that can be used to generate electricity with an attached generator [1] and [4].

This paper focuses on tidal-stream energy, which has been assessed in a growing number of published studies for different sites around the world using a variety of modelling techniques and tidal hydrodynamic models. A wide range of different bathymetric sources (e.g., global, regional and local bathymetry products, boat surveys and/or bathymetry charts) have been used to configure the underlying numerical model grids. Details of the studies that mention the specific bathymetric data sources they used, are summarised in Appendix A Table 1; a few of them will be revisited in the discussion section. Furthermore, different studies have considered different numbers and

combinations of tidal constituent when conducting energy resource assessments. For example, several past studies have investigated the variability of the available tidal-stream energy using just the M_2 tidal constituent e.g. for the Johnstone Strait, Vancouver Island [5], Masset Sound Haida Gwaii in Canada [6] and Pentland Firth, in the UK [7]. Therefore, here we consider it pertinent to conduct sensitivity testing comparing energy resource estimates calculated from numerical hydrodynamic simulations based on a variety of free global bathymetry products, and higher resolution datasets, and considering considered different numbers and combinations of tidal constituent. We focus on the Gulf of California, (Mexico) herein GC, building on an earlier study by [8].

The GC, located at the northwest of Mexico City (capital of Mexico) is about 1100 km in length. Furthermore, the GC is between 48 and 240 km in width between the Baja California peninsula and the mainland. The GC is divided into three main regions: (1) the northern region; (2) the central or Midriff region; and (3) the southern region. The bathymetry in the GC varies from around 200 m in the northern Gulf to 2,500-3,600 m depth at the entrance area with the Pacific Ocean. Peak spring tidal currents exceed 1.5 m/s around the Midriff Island in the Gulf of California [9] and [10]. Therefore, this region, where water depths are around 400 to 600 m, has potential for tidal-stream energy extraction. The first theoretical tidal-stream energy resource quantification was conducted recently by [8]. The GC is relatively deep, and diurnal tidal constituents are typically larger in the northern GC rather than at the entrance of the GC (Fig. 1) where water depths are approximately between 2000 and 3000 m depth. A study by [8] found that the resource characterisation in this region contrasts considerably from previously identified tidal-stream sites around the world, where water depth is typically less than 80 m. Currently developments of first-generation turbine requires tidal-stream flows > 2 m/s [11] and a maximum depth of < 80 m [12] [13].

The overall aim of this paper is to examine how choice of bathymetry product and number and combination of tidal constituents affects the quantification of the tidal-stream energy resource for the GC. We undertake sensitivity tests in which we estimate and compare the maximum theoretical undisturbed mean KPD and annual mean power output calculated from hydrodynamic model runs that used: (1) just GEBCO_2014 bathymetry data [14]; (2) just the ETOPO bathymetry data [15]; and (3) GEBCO_2014 data merged with higher resolution data from CICESE (The Centre for Scientific Research and Higher Education at Ensenada), for the upper part of the GC. We then consider how different numbers of tidal constituents affects the quantification of the tidal-stream energy resource for the GC. Crucially, and as explained in more detail below, we do not vary the number of tidal constituents at the model boundary when we run the model for a 1 month simulation; we just vary the number of tidal constituents we use to predict a complete year of tidal currents for estimating the tidal resource at different sites. The structure of the paper is as follows: in Section 2 we briefly describe the numeral model set up and configuration. The methodology is then outlined in Section 3. The results are presented in Section 4 and finally conclusions are given in Section 5.
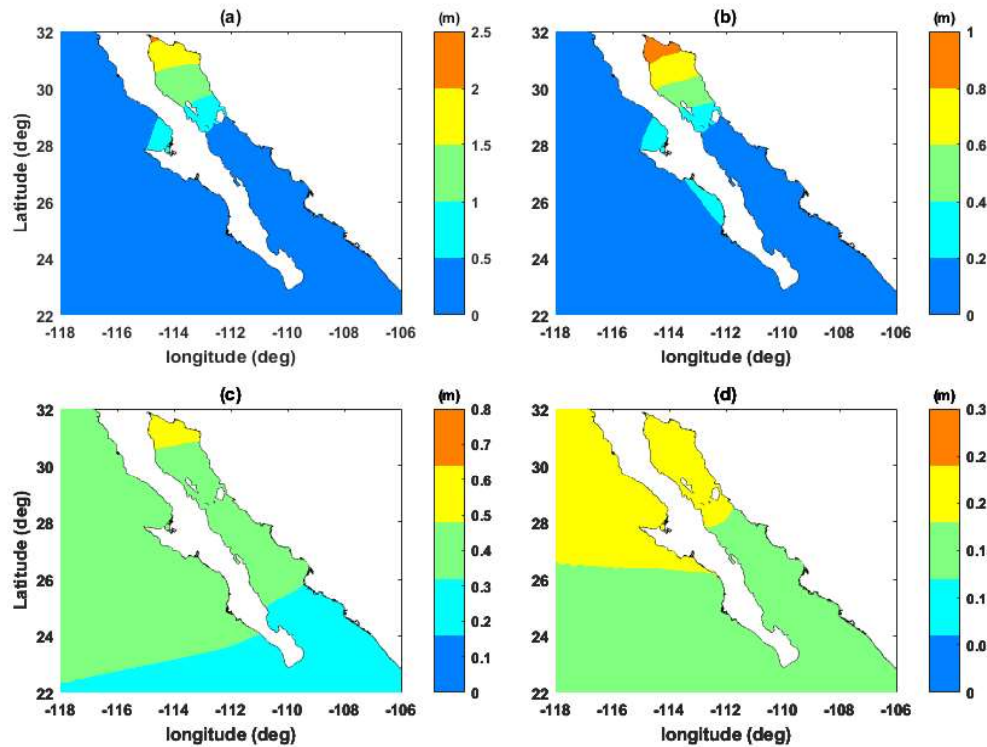
## 2. Gulf of California model configuration and validation

The GC hosts several deep basins, such as Tiburon, Delfin and Wagner, which are 400, 800 and 200 m deep, respectively. The Midriff region contains some important Islands, such as Smith, Salsipuedes, San Lorenzo, and San Esteban Islands. The biggest of the Gulf islands are Angel de la Guarda and Tiburon. The areas of most interest to this study is the region around the Midriff Islands in the central region, as a previous study indicates that currents in this region exceed 1.5 m/s [9] and hence, as first shown by [8], there is good potential for tidal-stream energy exploitation here, albeit in relatively deep (>200 m) water – hence likely floating turbine technology would be required for energy conversion.

A depth-averaged barotropic model of the GC was previously configured by [8] using the TELEMAC modelling suite [16]. Here we briefly describe the configuration and validation of that model. The TELEMAC modelling suite was chosen because of its: (1) computing performance - parallel processing, using the University of Southampton's supercomputer, IRIDIS, optimizing the simulation time; (2) the finite element method enabled variable mesh resolution to focus modelling effort in areas of interest; and (3) model inputs and outputs are compatible with a number of pre and post-processing software (e.g. Blue Kenue, Fudaa, MATISSE, Janet). TELEMAC has been recently utilised in previous energy resource assessments, for different regions, e.g. [17, 18 and 19]. The open ocean boundaries conditions were driven utilising only tidal levels (not velocities) predicted from the TPXO 7.2 dataset (see Reference [8] for further details). The computed tidal harmonics from the numerical simulation are then explored to examine the impact of their application to theoretical tidal resource

131 assessment within the annual yield estimate. The model mesh was built utilising the Blue Kenue software
132 developed by the National Research Council Canada (Fig. 2). The resolution of the mesh is ~60 km in the open
133 ocean and along the Pacific Ocean coast, subsequently increases to ~5 km at the entrance to the GC and to ~1 km
134 in the area of interest, around the Midriff Islands. It reduces to ~3 km resolution in the northern most reaches of
135 the GC.

136 The model was extensively validated against tide gauge and ADCP (acoustic Doppler current profiler)
137 measurements to ensure the accuracy of the predicted hydrodynamic conditions in the GC. Locations of the ADCP
138 data are shown in Table 1. Data for 11 tide gauge stations (see [8] for more details) located in the GC region and
139 along the Mexican Pacific ocean coastline were obtained from CICESE, along with current velocity data from 4
140 ADCP moorings. A variety of methods were utilised to assess the reliability of the model performance in
141 accurately reproducing observed tidal levels and tidal currents. Therefore, modelled and observed tidal level and
142 currents were compared, along with the amplitude and phase for the main tidal constituents (M_2, S_2, N_2, K_1, O_1,
143 P_1, Q_1), calculated using the T_TIDE MATLAB software package [20]. Additionally, percentage errors were
144 calculated to quantify the model's ability to reproduce the hydrodynamic conditions (see [8] for all the metrics of
145 the model validation).

146 In this paper we focus on carrying out two main sensitivity tests focusing on different bathymetries and choice of
147 tidal constituents. However, when setting up the model originally, we also undertook numerous sensitivity tests
148 to assess model perform for a range of different domain areas, mesh resolutions and using different uniform and
149 spatially varying bottom friction coefficients. The grid resolution was gradually increased, to quantify if validation
150 against observations improved with higher resolution. With higher resolution model run times increase
151 significantly, so there is a balance between capturing approach resolutions and ensuring the simulations can be
152 made in appropriate time-scales. Numerous sensitivity tests were undertaken to assess model perform using a
153 range of uniform and spatially varying bottom friction coefficients and the different friction law options that are
154 available in TELEMAC (e.g., Nikuradse, Manning and Chézy formula). Overall, differences between the model
155 predictions and measurements were lowest when the Manning's law was used to define friction and when a
156 spatially uniform value of 0.030 ($s/m^{1/3}$) was used. In addition, the accuracy of the model predictions were
157 sensitive to the resolution and quality of the bathymetry data interpolated onto the model grid (see Appendix B
158 which includes the steering file for the model settings in TELEMAC 2D [21]).

159

160
161
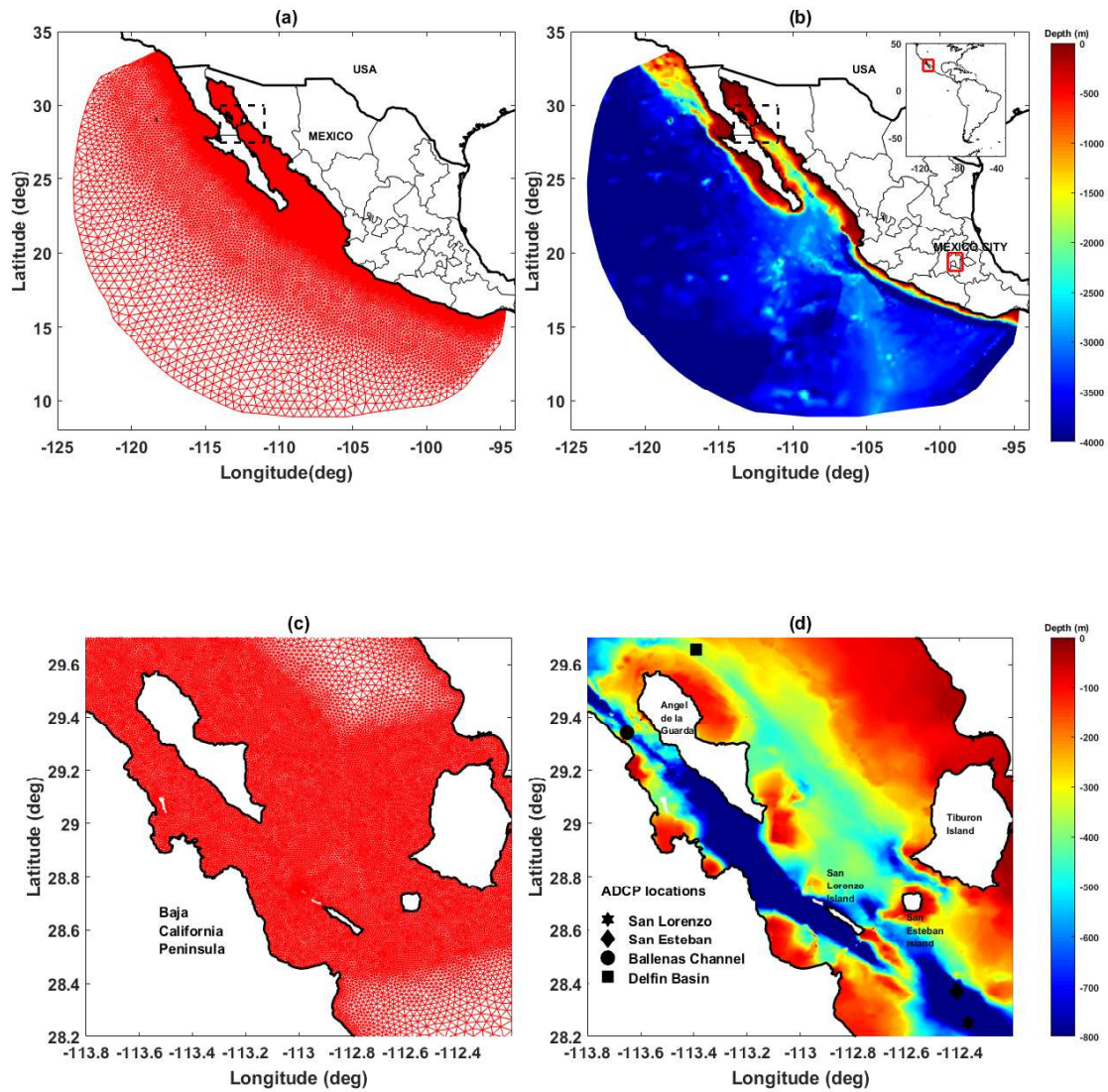
162 **Fig. 2** Model grid for the: (a) whole domain area; and (c) just the Midriff area. Combined bathymetry used
163 (GEBCO_2014 and CICESE) for the: (b) whole domain area; and (d) just the Midriff area, ADCP locations are
164 given as black symbols, which correlate to the mooring locations in Table 1 as (1) San Lorenzo, (2) San
165 Esteban, (3) Ballenas Channel, (4) Delfin Basin shown as pentagram, diamond, circle and square respectively.

166

3. Sensitivity tests to assess the theoretical energy

168 First, we undertake sensitivity tests in which we estimate and compare the peak tidal currents, maximum
169 theoretical undisturbed mean KPD (Kinetic Power Density) and annual mean power output calculated from the
170 hydrodynamic model, but with the mesh depths defined using different bathymetry products. We ran two
171 simulations first, using just bathymetry data from two well-known and well-used sources: (1) General Bathymetry
172 Chart of the Oceans, 2014 version (GEBCO_2014) [14]; (2) ETOPO bathymetry data [15], which are available at
173 resolutions of ~900 and ~775 m, respectively. A third run used the GEBCO data merged with the higher resolution
174 single beam echo sounder data from CICESE (the Centre for Scientific Research and Higher Education at
175 Ensenada, https://www.cicese.edu.mx/). The higher resolution (~450 m) bathymetry data covers the northern

6

176   (north of 27° to 32°) GC. The extent of the bathymetry dataset is shown in Fig. 3 for the GC, and the Midriff

177   region of the GC and the northern GC. The higher resolution bathymetry dataset was combined with GEBCO

178   using a *merge* function in ArcGIS software which combined multiple inputs of datasets even though the data

179   overlap. Consequently, none of the points from either the GEBCO_2014 or CICESE data sets were omitted or

180   altered. A cross-sectional from the central region of the GC is shown in Fig. 4, highlighting the main differences

181   for the three different products utilized in this work. The three different model bathymetries within the Midriff

182   region are shown in Fig. 5, and can be seen to vary between the main islands in this area.

183   Second, we examined how current speeds, mean kinetic power density and annual mean power estimates varied

184   depending on which tidal constituents were used to predict tidal levels. The open ocean boundaries were driven

185   using tidal levels predicted from the TPXO 7.2 dataset [22 and 23]. The ocean model was always forced by the

186   eight main diurnal and semi-diurnal constituents (M_2, S_2, N_2, K_1, O_1, P_1, Q_1), three nonlinear constituents (M_4,

187   MS_4, MN_4), and two long period constituents (Mf, Mm), at 1/4° resolution. Our high-resolution grid simulates the

188   interaction among constituents, thus resolving higher harmonics (e.g., M_4, M_6 and M_8). We ran the model for a 1-

189   month period and carried out a harmonic analysis on the predicted tidal levels, using T_TIDE in MATLAB. To

190   avoid computational constraints, we then used the tidal current harmonics to predict the tidal currents for a full

191   year. First, we estimated the peak current speeds, mean kinetic power density and annual mean power, considered

192   all the 29 tidal constituents returned by the T_TIDE harmonic analysis [8]. Then, the peak current speeds, KPD

193   and the annual maximum theoretical undisturbed mean power, were calculated considering: (1) only the M_2 tidal

194   constituent; (2) only the S_2 constituent, and the finally (3) the M_2 plus S_2 constituent.

195
196
197
198
199
200
201
202
203
204
205
206
207
208
209
210
211
212
213
214
215
216
217
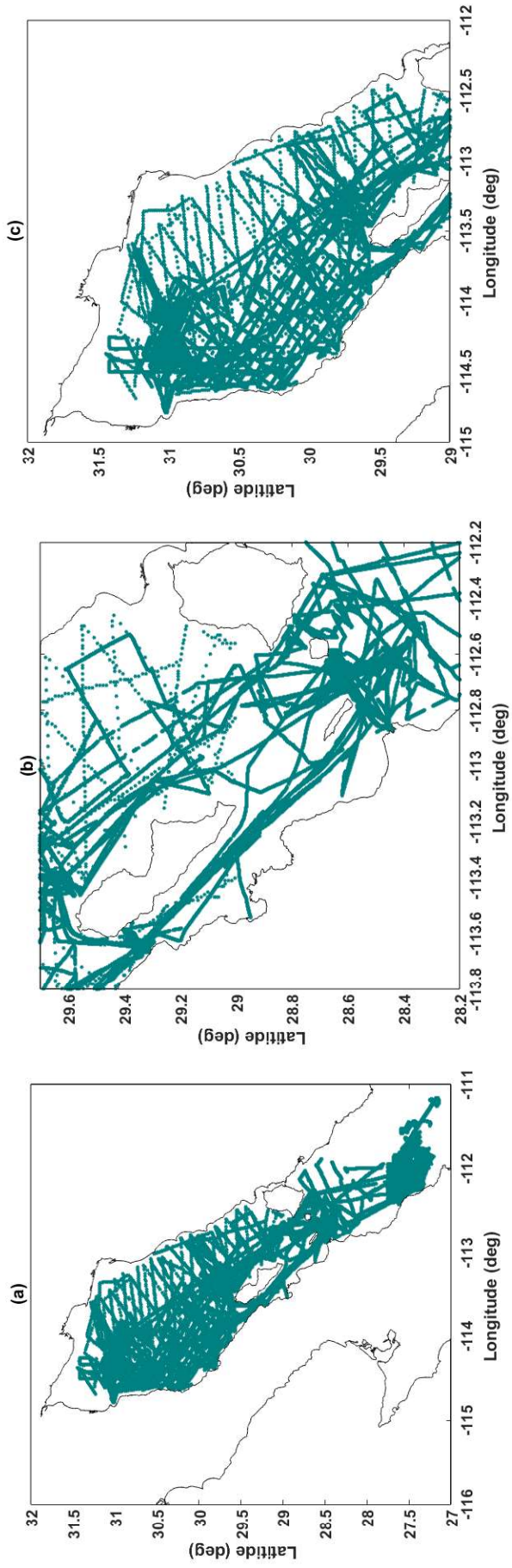
Fig. 3 Bathymetry survey by CICESE research centre for the: (a) Gulf of California; (b) midriff area; and (c) northern Gulf of California.
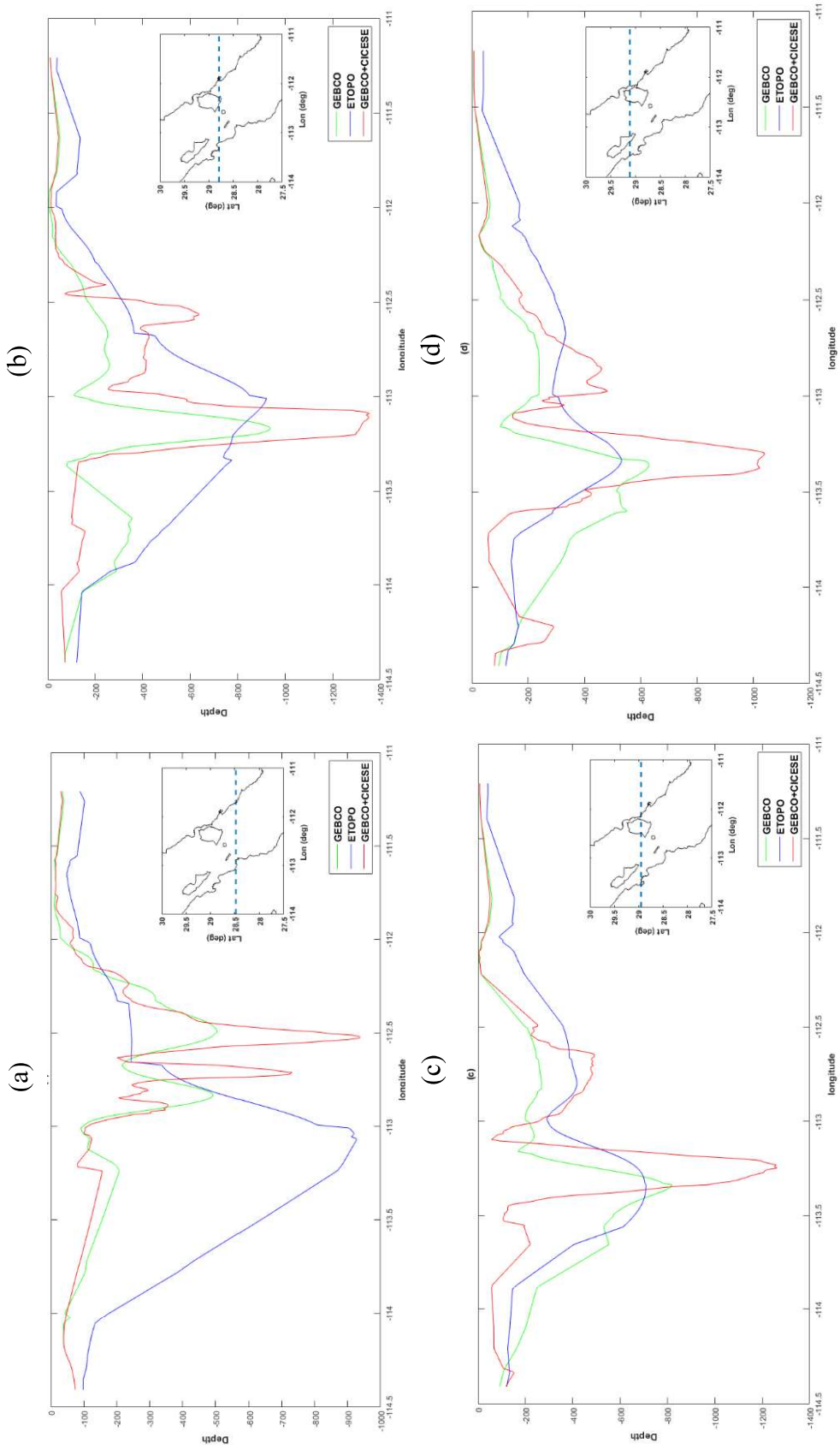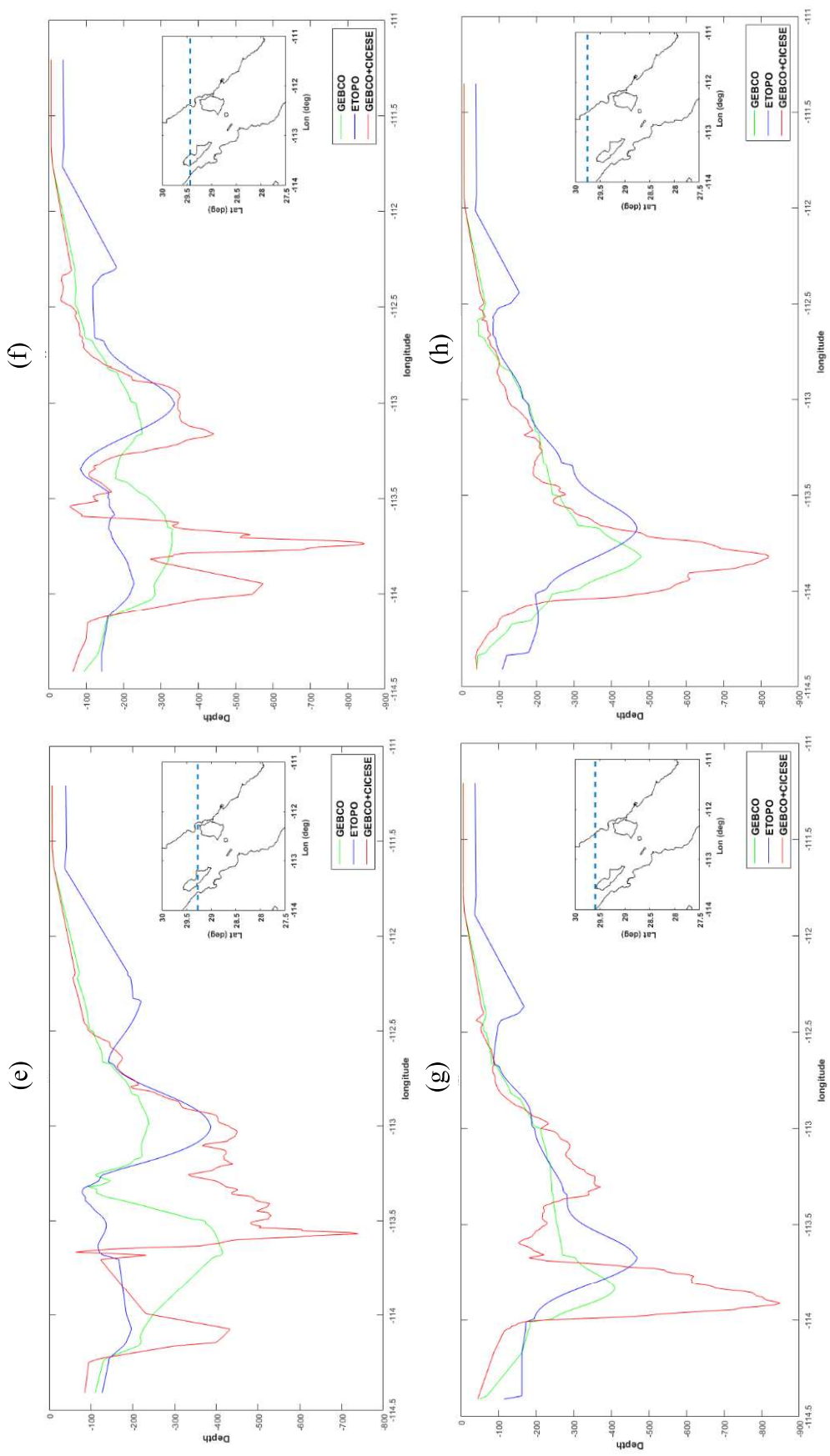
Fig. 4. Bathymetric cross-sectional profile (location showed in inlay in panel a) considering: just GEBCO, just ETOPO and GEBCO_2014 merged with CICESE, data sets, Y axis is depth in m.

219
220
221
222
223
224
225
226
227
228
229
230
231
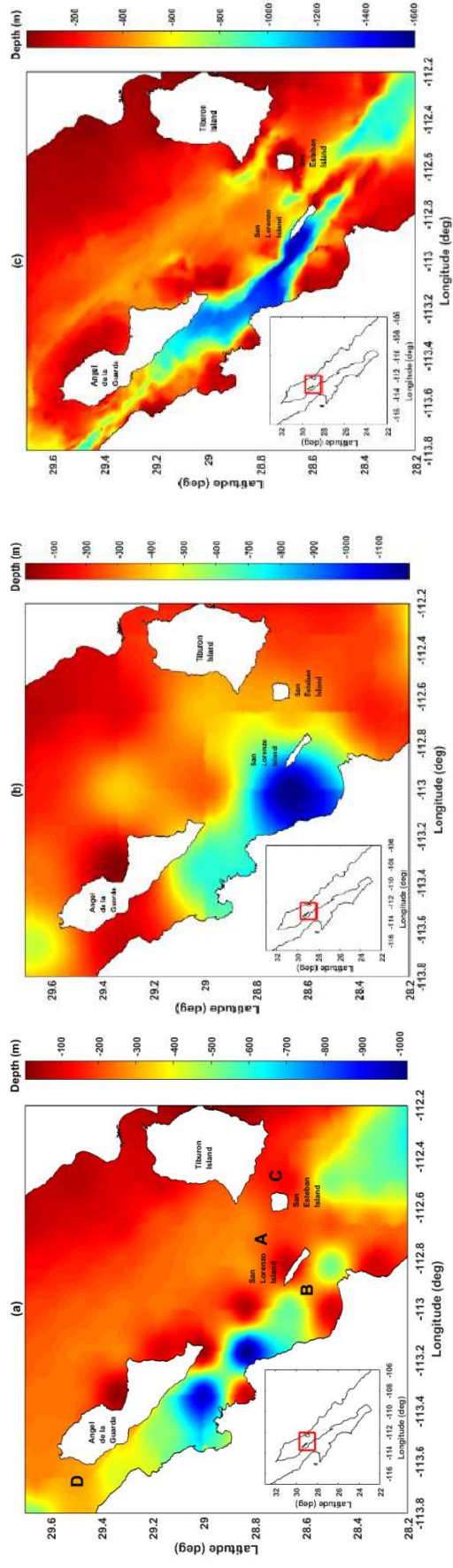
Fig. 5 Model bathymetry created using: (a) just GEBCO_2014 data, (b) just ETOPO data and (c) GEBCO_2014 merged with CICESE data, for the Midriff area.

4. Results

The results are presented in three sub-sections below. The first sub-section discusses the model validation, obtained using the three different bathymetries. The second and third sub-sections describe the results of the bathymetry and tidal constituent sensitivity tests, respectively.

4.1 Model validation

This section presents the GC model validation and how the validation varies across the three different bathymetry products (Fig. 6) Model validation is important as it gives confidence in the model's ability to reproduce the tidal flows in the region with reasonable accuracy. Percentage errors and RMSE were used to quantify the validation for the three different bathymetry products utilized within the model simulations, at the 11 tide gauge stations (see [8] for the tide gauge locations), and are listed in Table 2 and Table 3, respectively. The largest percentage error is at La Paz (11.5 %) using the ETOPO bathymetry product, while the smallest errors are at Ensenada (1.1 %, 1.2 % and 1.2 %) using the three different products respectively (GEBCO, ETOPO, and GEBCO merged with CICESE). The mean percentage error across all sites is 5 % using the combined bathymetry data. The percentage errors are largest at Guerrero Negro (9.6 %, where the tide gauge is in an enclosed bay), Cabo San Lucas (3 %), Manzanillo (6.1 %) and Acapulco (7.7 %). However, the mean percentage error overall for GEBCO_2014 and CICESE merged bathymetry product was slightly better at around 4 to 6 %. Therefore, the model provides better representation of tidal levels across all the domain region using the combined GEBCO_2014 and CICESE datasets.

A comparison between eastward (u) and northward (v) velocity components for the 4 ADCP locations utilising the three bathymetry products are shown in Fig. 7 and 8 respectively. Graphically, significant differences can be seen when using just the GEBCO_2014 and ETOPO products. For u and v current components, smaller predicted current speeds were found at San Lorenzo (Fig. 7a and 8a) and San Esteban Island (Fig. 7b and 8b) while closer approximations of the current speeds were predicted at Ballenas channel (Fig. 6g and 7g) and Delfin Basin (Fig. 7j and 8j) using GEBCO_2014 only. In contrast, both velocity components were overestimated while using ETOPO bathymetry data only within Ballenas channel (Fig. 7h and 8h) and Delfin basin (Fig. 7k and 8k).

266 **Table 1** ADCP location and deployment details

Site Name	Depth device deployment/ water depth in m	Longitude (decimal °)	Latitude (decimal °)
San Lorenzo	395/410	-112.37	28.25
San Esteban	577/588	-112.41	28.37
Ballenas Channel	578/595	-113.38	29.20
Delfin	337/354	-113.23	29.38

267

268

269 **Table 2** Statistic percentage errors calculated of tidal level constituents for the 11 tide gauges stations using
270 different bathymetry products.

Site number	Site Name	% Error GEBCO	% Error ETOPO	% Error GEBCO merged with CICESE
1	Ensenada	1.1	1.2	1.2
2	San Quintin	4.4	4.8	4.5
3	Isla Cedros	4.3	4.5	4.4
4	Guerrero Negro	9.4	8.9	9.6
5	Cabo San Lucas	2.10	2.7	3.0
6	La Paz	11.2	11.5	10.9
7	Loreto	6.3	4.5	5.9
8	Bahia de los Angeles	7	6.8	3.0
9	San Felipe	5.1	3.3	3.8
10	Manzanillo	6	6	6.1
11	Acapulco	7.4	7.4	7.7
All	**Mean**	**5.4**	**5.6**	**5.0**

271

272

273 **Table 3** RMSE calculated of tidal level constituents for the 11 tide gauges stations using different bathymetry
274 products.

Site number	Site Name	RMSE GEBCO	RMSE ETOPO	RMSE GEBCO merged with CICESE
1	Ensenada	0.03	0.03	0.03
2	San Quintin	0.11	0.11	0.11
3	Isla Cedros	0.1	0.1	0.1
4	Guerrero Negro	0.25	0.24	0.26
5	Cabo San Lucas	0.04	0.04	0.06
6	La Paz	0.19	0.18	0.19
7	Loreto	0.08	0.06	0.08
8	Bahia de los Angeles	0.22	0.22	0.09
9	San Felipe	0.33	0.21	0.25
10	Manzanillo	0.07	0.07	0.07
11	Acapulco	0.07	0.07	0.07
All	**Mean**	**0.13**	**0.12**	**0.11**

275
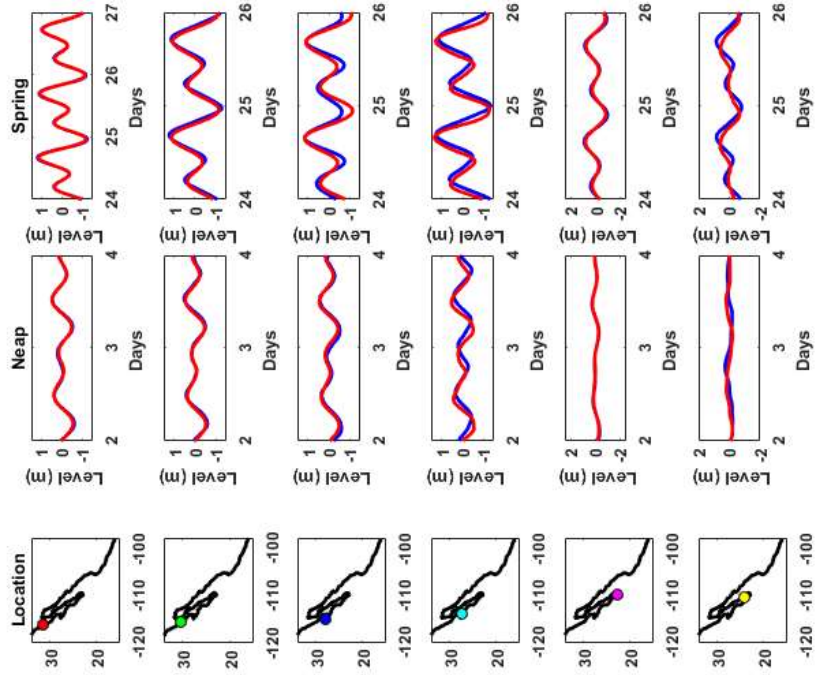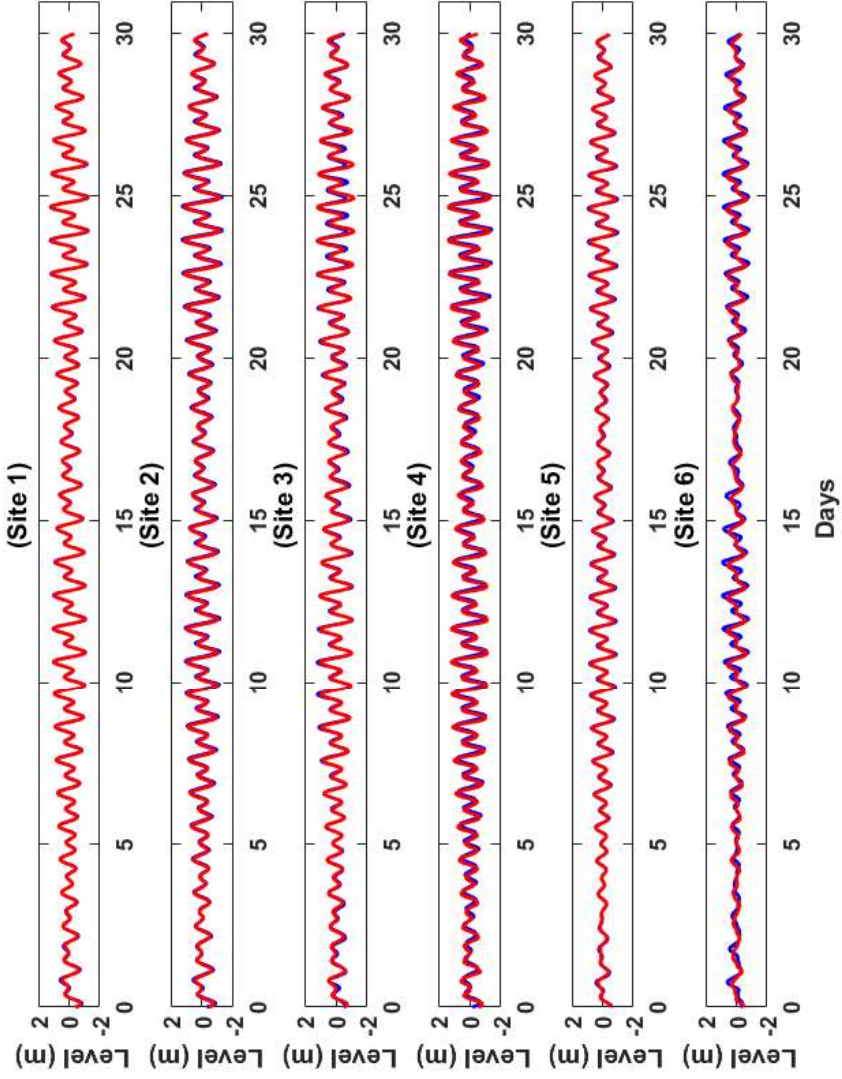
276

277

278

279
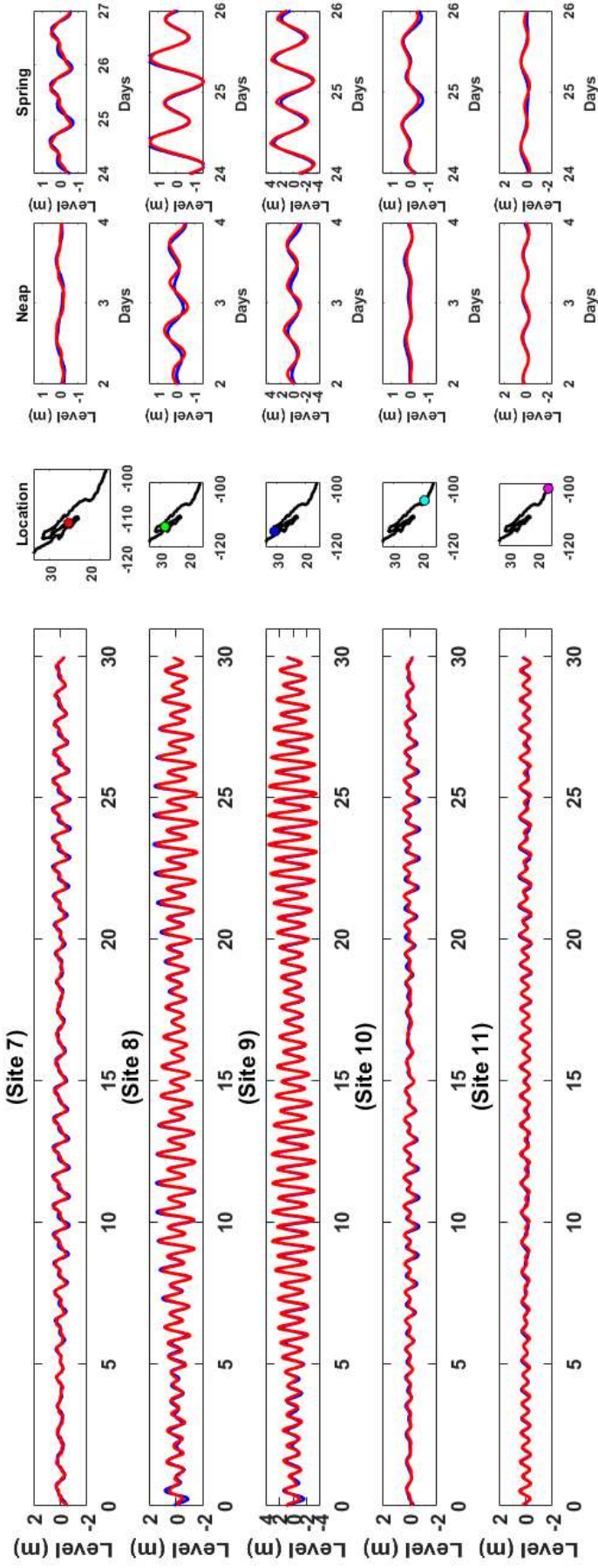
Fig. 6 Comparison of the measured (blue) and predicted (red) tidal time-series at: (1) Ensenada; (2) San Quintin; (3) Isla Cedros; (4) Guerrero Negro; (5) Cabo San Lucas (6) La Paz; (7) Loreto; (8) Bahia de los Angeles; (9) San Felipe; (10) Manzanillo; (11) Acapulco. All plots use the model run for the period from 27 November 2015 to31 December 2015 using the GEBCO data merged with the higher resolution data from CICESE, for the northern Gulf of California showed on figures 3a, b and c.

16
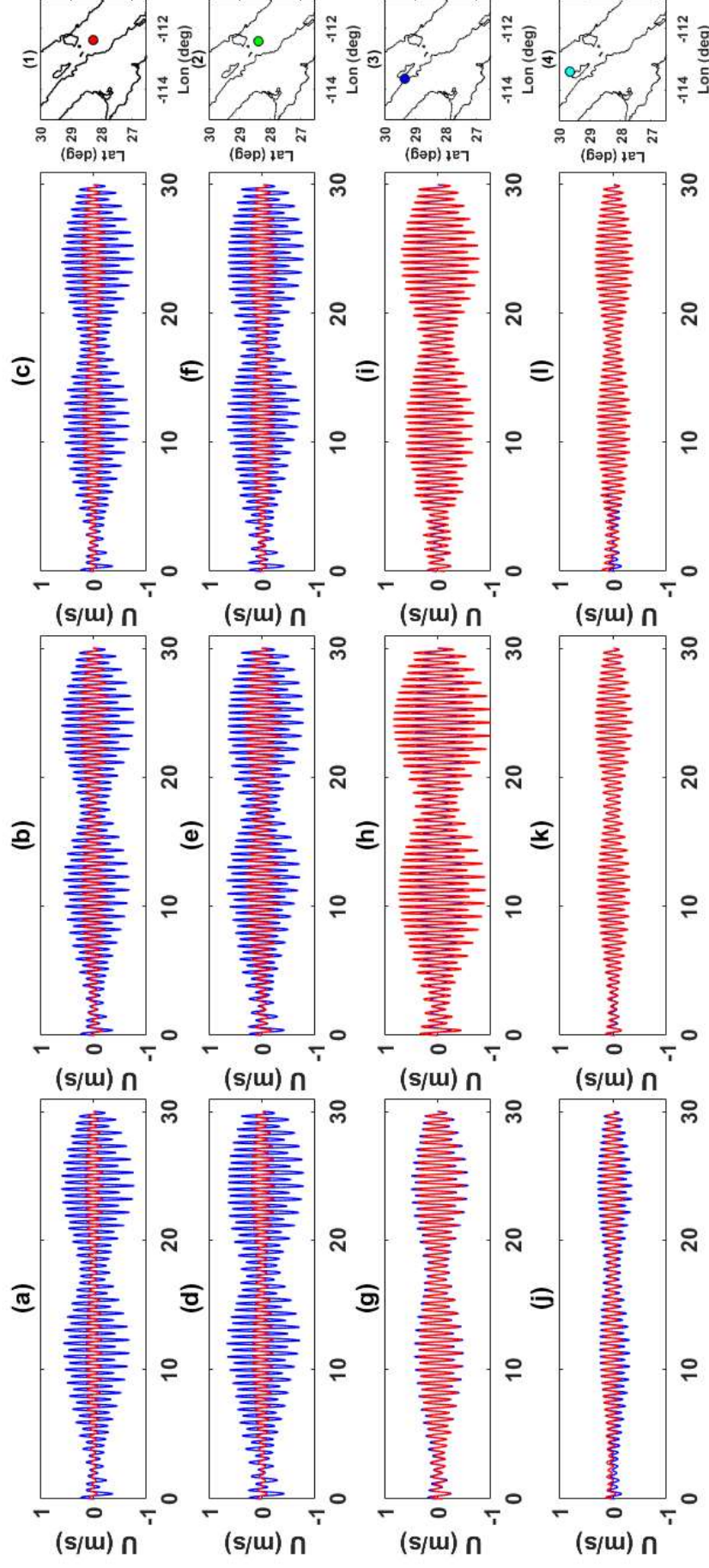
Fig. 7 Comparison of the observations (blue) and model results (red) for the u velocity component (eastward velocity) with different bathymetry products as follows: (a,d,g,j) just GEBCO data; (b,e,h,k) just ETOPO data; and (c,f,i,l) GEBCO merged with CICESE; at: (a,c) San Lorenzo; (d,e,f) San Esteban; (g,h,i) Ballenas Channel; and (j,k,l) Delfin Basin. All plots use the model run for the period from 27 November 2015 to 31 December 2015 and comparison them with observations.

288
289
290
291
292
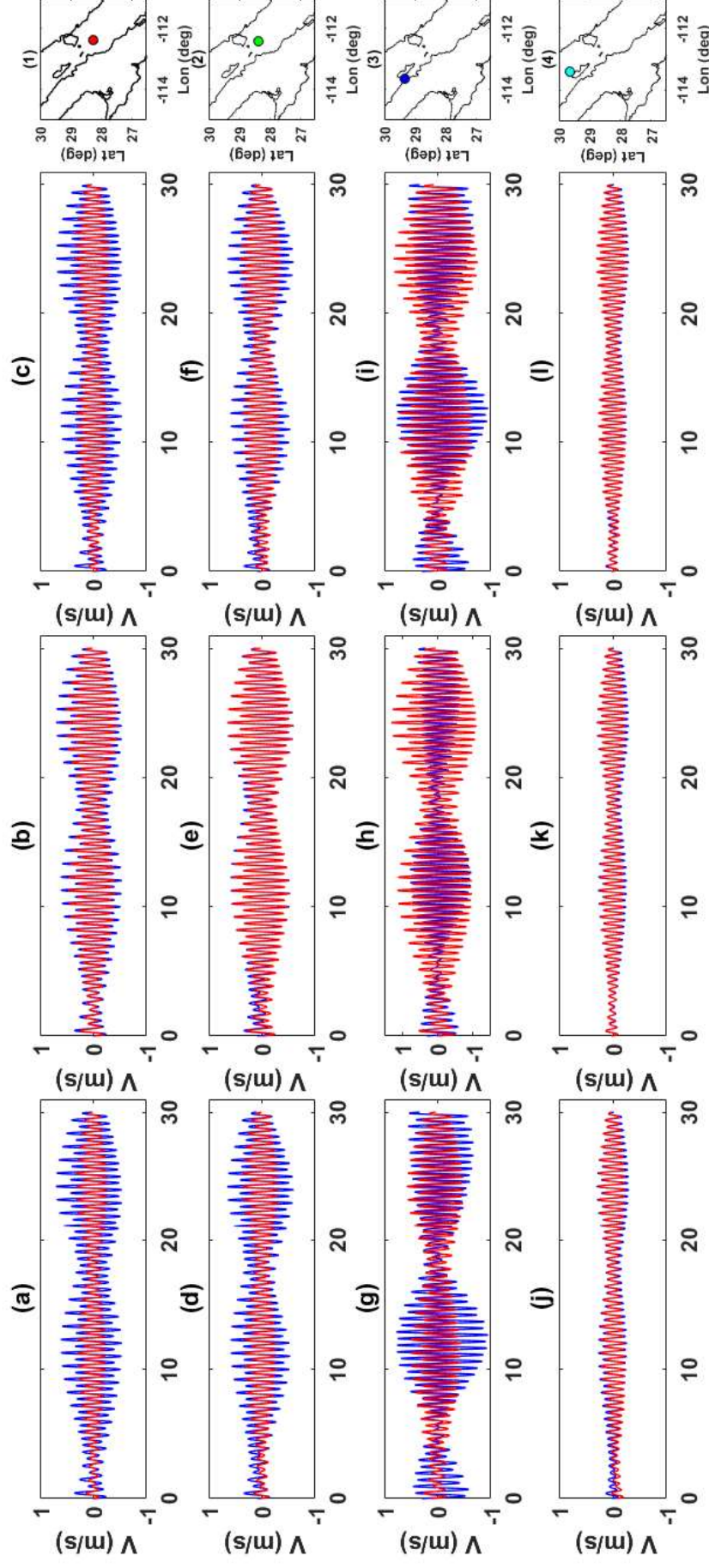
Fig. 8 Comparison of the observations (blue) and model results (red) for the v velocity component (northward velocity) with different bathymetry products as follows: (a,d,g,j) just GEBCO data; (b,e,h,k) just ETOPO data; and(c,f,i,l) GEBCO merged with CICESE; at: (a,c) San Lorenzo; (d,e,f) San Esteban; (g,h,i) Ballenas Channel; and (j,k,l) Delfin Basin. All plots use the model run for the period from 27 November 2015 to 31 December 2015 and comparison them with observations.

293
294
295
296
297

Percentage errors and RMSE were calculated to quantify the model skill, for each of the three bathymetries, at the 4 ADCP locations and these are listed in Table 4 and Table 5 (see Fig 2d for the ADCP locations). The largest error of the v component is in Ballenas channel using GEBCO (17.0 %) and ETOPO (26.1 %) bathymetric data on their own. Ballenas channel is relatively deep at around 800 to 900 m, and we assume that the bathymetry products influence negatively the predicted u and v component. The smallest errors for the u and v components are at Delfin basin; which are 2.7 % and 3.7 %, respectively, when using the combined GEBCO and CICESE data. Therefore, we can conclude that a higher resolution bathymetry data can contribute significantly to improve the current validation. In summary, the model validation improved when the higher resolution bathymetry data for the Midriff region (obtained from CICESE with a resolution of~450 m) was merged within the GEBCO dataset (~900 m resolution) (Fig. 6e,f) compared to just using GEBCO (Fig. 7a,b) or ETOPO data alone (Fig. 8 c,d). In addition, the absolute current velocity comparisons are shown in Table 6. Furthermore, amplitude and phases of the u and v velocity components utilising M_2 and S_2 model simulation are shown in table 7 and 8 respectively. Amplitude and phases results were estimated using the merged bathymetry data (GEBCO_2014 merged with CICESE).

Table 4: Percentage error of u and v velocity components using different bathymetry products

Site Name	% Error GEBCO u	% Error GEBCO v	% Error ETOPO u	% Error ETOPO v	% Error GEBCO merged with CICESE u	% Error GEBCO merged with CICESE v
San Lorenzo	13.81	11.38	11.82	5.89	11.3	8.5
San Esteban	14.77	9.20	12.55	4.31	11.5	6.7
Ballenas Channel	3.25	16.97	15.28	26.12	6.7	25.0
Delfin	8.50	5.99	2.92	3.28	2.7	3.7
Mean	**10.08**	**10.88**	**10.64**	**9.90**	**8.04**	**11**

319 **Table 5:** RMSE error of u and v velocity components using different bathymetry products

Site Name	RMSE GEBCO u	RMSE GEBCO v	RMSE ETOPO u	RMSE ETOPO v	RMSE GEBCO merged with CICESE u	RMSE GEBCO merged with CICESE v
San Lorenzo	0.18	0.14	0.16	0.07	0.18	0.12
San Esteban	0.21	0.11	0.18	0.05	0.19	0.10
Ballenas Channel	0.03	0.29	0.16	0.45	0.09	0.32
Delfin	0.05	0.03	0.02	0.02	0.02	0.03
Mean	**0.12**	**0.15**	**0.13**	**0.15**	**0.12**	**0.14**

320

321 **Table 6:** Comparison of the measured and predicted absolute current velocity in (m/s) for the bathymetry
322 products used on this study.

Site Name	Absolute current velocities (observations)	Absolute current velocities ETOPO	Absolute current velocities GEBCO	Absolute current velocities GEBCO merged with CICESE	RMSE ETOPO	RMSE GEBCO	RMSE GEBCO merged with CICESE
San Lorenzo	0.35	0.22	0.12	0.16	0.14	0.22	0.20
San Esteban	0.37	0.26	0.14	0.19	0.11	0.22	0.18
Ballenas Channel	0.38	0.57	0.26	0.44	0.32	0.16	0.20
Delfin	0.16	0.16	0.12	0.18	0.01	0.05	0.03

323

324

Table 7: Comparison of the measured and predicted u and v velocity amplitudes and phases at the four ADCP sites for M_2 tidal constituent.

Site Name	Amplitude M_2 model (m)		Amplitude M_2 Observations (m)		Phase M_2 model (°)		Phase M_2 Observations (°)	
	u	v	u	v	u	v	u	v
San Lorenzo	0.009	0.013	0.030	0.003	210	139	178	186
San Esteban	0.010	0.015	0.039	0.003	220	139	222	169
Ballenas Channel	0.029	0.031	0.023	0.005	221	141	229	181
Delfin	0.014	0.011	0.013	0.001	215	121	210	207

Table 8: Comparison of the measured and predicted u and v velocity amplitudes and phases at the four ADCP sites for S_2 tidal constituent.

Site Name	Amplitude S_2 model (m)		Amplitude S_2 Observations (m)		Phase S_2 model (°)		Phase S_2 Observations (°)	
	u	v	u	v	u	v	u	v
San Lorenzo	0.0091	0.0132	0.0303	0.0033	210	139	178	186
San Esteban	0.0104	0.0156	0.0393	0.0036	220	139	222	169
Ballenas Channel	0.0297	0.0316	0.0239	0.0056	221	141	229	181
Delfin	0.0146	0.0115	0.0134	0.0011	215	121	210	207

There are a few cases, at particular sites, when the GEBCO_2014 merged with CICESE bathymetry does not give the lowest root mean square error (RMSE) difference listed in Tables 3, 4, 5 and 6. However, when the RMSEs are averaged across all the 11 tide gauge sites, or all 4 current sites, then the GEBCO_2014 merged with CICESE bathymetry consistently gives the best overall agreement between the observed and measured time-series. The averaged RMSE errors are listed in the last row of Tables 3, 4, 5 and 6. In all cases it can be seen that the GEBCO_2014 merged with CICESE bathymetry consistently gives the best agreement.

4.2 Bathymetry sensitivity tests

Next, we compare the maximum current speeds and the estimated 'theoretical' power from the three different bathymetry simulations, for the Midriff region (Fig. 4c and 5c). Current speeds vary significantly between the three different bathymetry products within the four main regions where current speeds exceed 1 m/s (Fig. 9). The largest current speeds were localised within San Lorenzo Passage (channel between San Lorenzo and San Esteban Island) reaching a maximum of about 2.4 m/s in the deeper-water (~500 m) for the combined GEBCO and CICESE bathymetry. In contrast, when using just GEBCO or ETOPO bathymetry products, the current speeds in this channel reduce to around 1.2 m/s and 0.8 m/s, respectively. Similarly, in the region of Ballenas channel (channel between Angel de la Guarda Island and the Baja California Peninsula) relatively large differences were found. Using the combined bathymetry dataset (Fig. 9c) the flow speed was estimated to be around 1 m/s, whereas using GEBCO data only (Fig. 9a) the current speed reduced to 0.5 m/s. However, the use of ETOPO bathymetry overestimated the current speed within Ballenas channel at around 1.8 m/s (Fig. 9b).

353
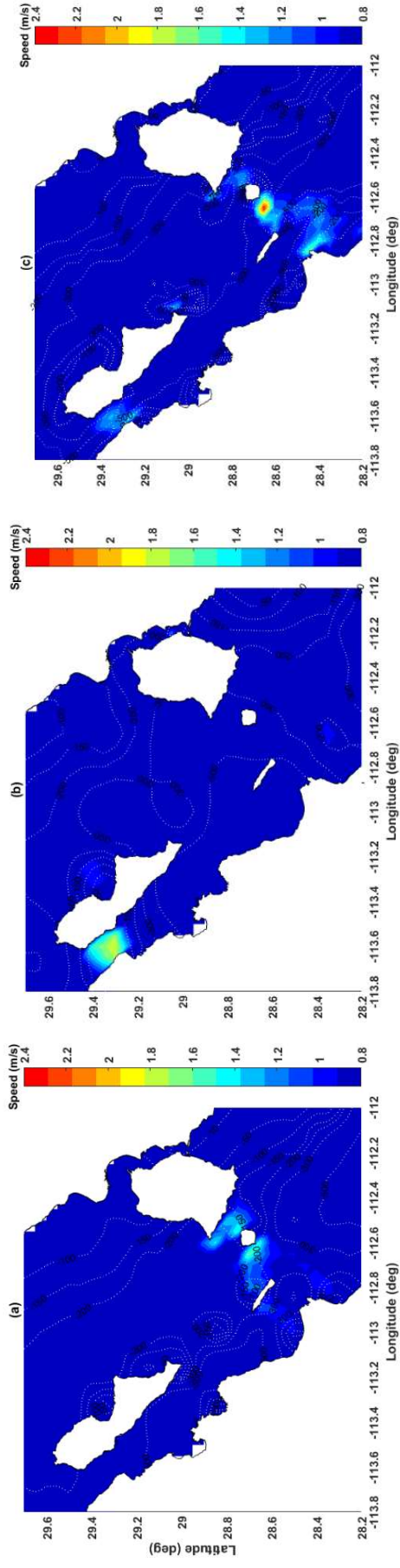
Fig. 9 Maximum current speed calculated using: (a) just GEBCO_2014 data, (b) just ETOPO data (c) GEBCO_2014 merged with CICESE. Bathymetric contours are superimposed in m. All figures include the 29 tidal constituents originally used the model set up by [8].

The annual mean power is significantly underestimated when using just the GEBCO_2014 or ETOPO bathymetry data sources on their own for the Midriff region (Fig. 10). For the region with fastest current speeds, San Lorenzo Passage, the annual mean power was 150 MW and 20 MW when using the GEBCO_2014 and ETOPO bathymetries, respectively (Fig. 10a and c. Whereas the annual mean power was calculated as ~200 MW when using the bespoke dataset (Fig. 10f). Similarly, in the region between San Lorenzo and the Baja California peninsula (Marker B on Fig. 5a) where the currents speeds are around 1.4 m/s, the annual mean power was estimated to be around 160 MW when using the combined bathymetry products whereas the resource reduces approximately to 80 MW and 40 MW when using GEBCO_2014 and ETOPO runs respectively. In the case of Ballenas channel, the annual mean power was estimated to be 150 MW when using the combined bathymetry data, however, the annual mean power was significantly overestimated at around 180 MW when using just ETOPO bathymetry (Table 9).
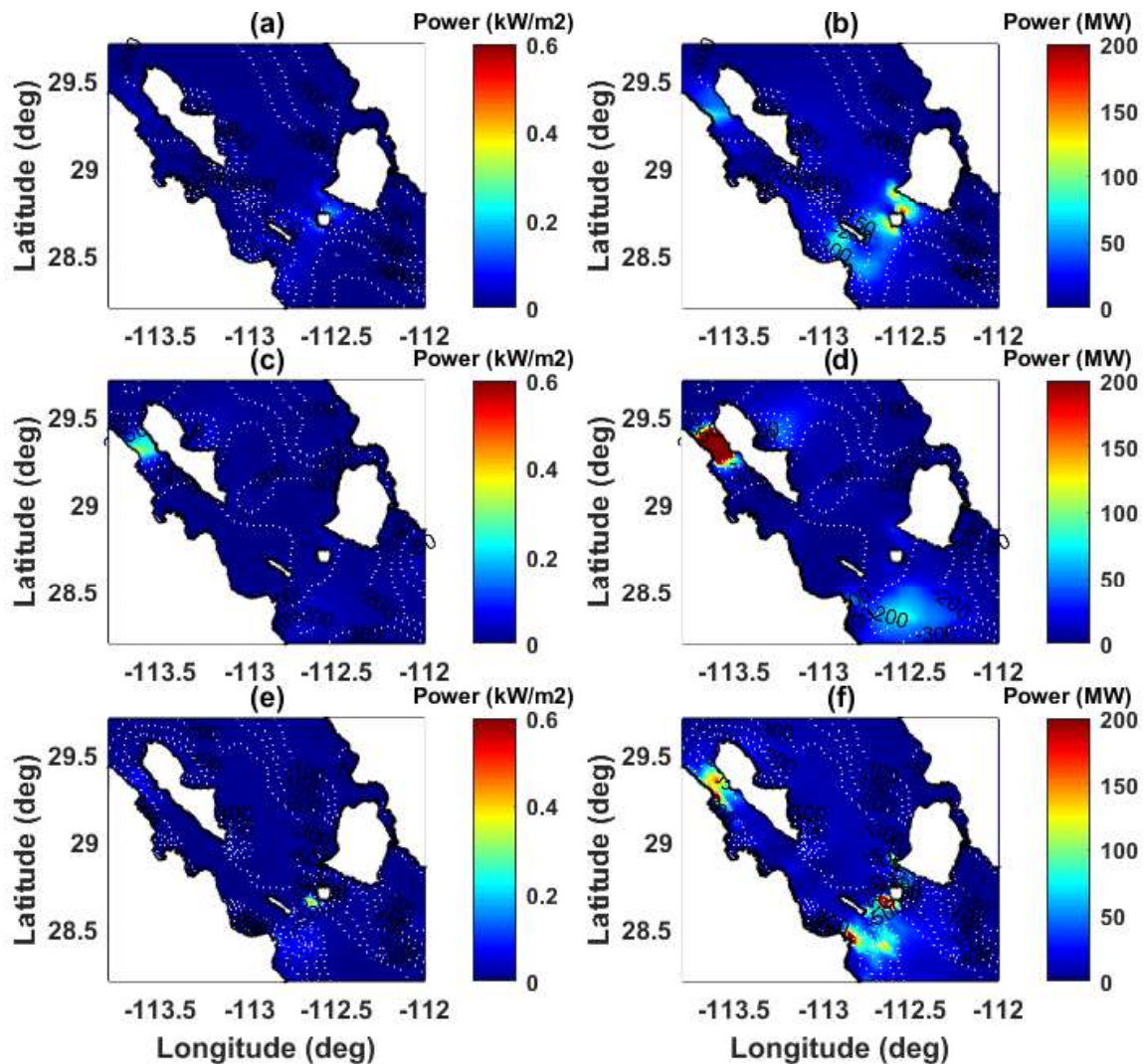
Fig. 10 (a,c,e) Annual mean kinetic power density, (c,f,i) Annual mean power and (b,d,f), (a,b) just GEBCO_2014 data; (c,d) just ETOPO data and (e,f) GEBCO_2014 merged with CICESE, for the Midriff region. Bathymetric contours superimposed in m above.

373

374

375

376

377

378

379

380

381

382

383

384

385

386

387

388

389

390

391

392

393
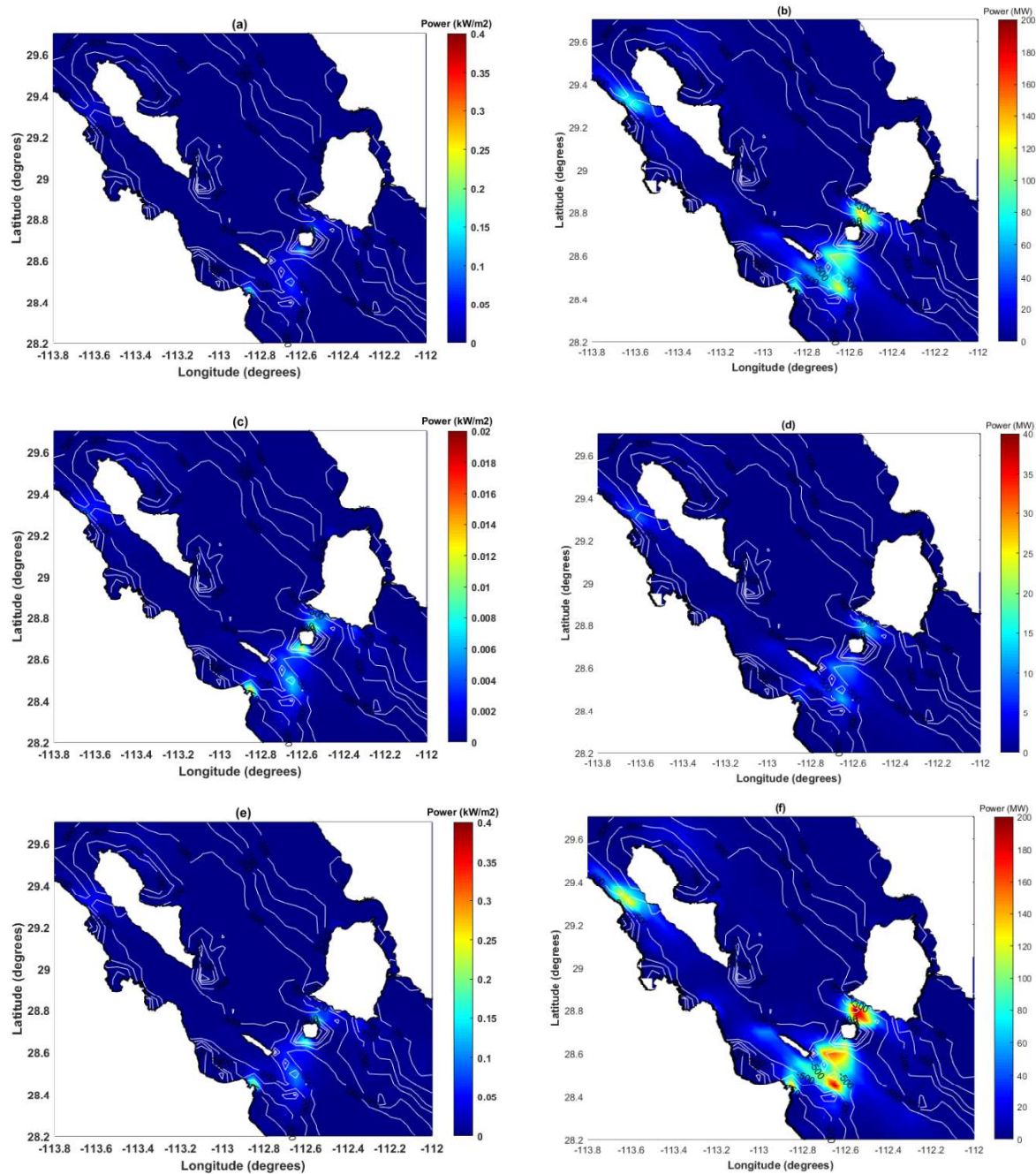
394 **Fig. 11** Annual mean kinetic power density (a) just the M_2 constituent, (c) S_2 constituents (e) M_2 plus S_2
395 constituents. Annual theoretical mean power for (b) just the M_2, (d) S_2 constituents (f) M_2 plus S_2 constituents.
396 All plots use the GEBCO_2014 data merged with the higher resolution data from CICESE, for the Midriff region,
397 for the model bathymetry. Bathymetric contours superimposed in m above.

398

399

400

401

402

Table 9: Annual mean theoretical power (MW) by location using different bathymetry products. Marker Fig. 5a (A) San Lorenzo Passage. (B) channel between the Baja California Peninsula and San Lorenzo, (C) Channel between San Esteban and Tiburon Island and (D) Ballenas Channel between the Baja California Peninsula and Angel de la Guarda Island

Site Marker	GEBCO	ETOPO	GEBCO merged with CICESE
A	~120	~20	~200
B	~80	~40	~160
C	~140	~10	~40
D	~70	~180	~150

4.3 Tidal constituent sensitivity tests

In the next stage of testing, we considered how different numbers and combinations of tidal constituents affect the quantification of the tidal-stream energy resource for the GC. Note again, that we did not vary the number of tidal constituents used to force the model boundary; we only varied the number of tidal constituents used to predict a year of tidal currents used for quantifying the tidal-stream energy resource. The results of these tests are shown in Fig.11. The annual mean KPD was first estimated using only the M_2 tidal constituent (Fig. 11a). The annual mean KPD was calculated of around 0.18 to 0.08 kW/m², while the maximum value reached was calculated as ~0.25 kW/m² where the fastest currents were occurring (San Lorenzo Passage). Furthermore, significant differences were found where the annual maximum theoretical undisturbed mean power was calculated utilising M_2 and S_2 on their own in San Esteban Passage. Using the M_2 tidal constituent, the estimation of the annual power is between 90 and 100 MW (Fig. 11b), while using just the S_2 tidal constituents the annual power reduced significantly to around 15 to 20 MW (Fig. 11d). This is because S_2 generally is around half that of M_2 in the region.

Similarly, the annual mean power was calculated using M_2 plus S_2, where the results indicated an annual mean power range of 140 to 150 MW (Fig. 11f). When considering predicted tidal levels, calculated using all 29 tidal constituents, the maximum annual mean was calculated in San Esteban Passage was ~200 MW. The mean annual power reduces significantly to around 70% using just M_2 plus S_2 tidal constituent from approximately 200 MW to 140-150 MW. The annual mean power in San between Lorenzo Island and the Baja California peninsula (Marker B on Figure 5a) was calculated between 60 to 70 MW when using the M_2 tidal constituent, whereas the annual mean power increased by almost the double (approximately 120 to 130 MW) when using the M_2 plus S_2 tidal constituents. Similarly, in the case of Ballenas (Marker D on Fig. 5a) the annual mean power reduces from 60 to 70 MW when using only M_2 to 120 to 130 MW when using M_2 plus S_2 (Table 10).

434 **Table 10:** Annual mean theoretical power (MW) by location using different tidal constituents with GEBCO
435 merged with CICESE. (A) San Lorenzo Passage. (B) channel between the Baja California Peninsula and San
436 Lorenzo, (C) Channel between San Esteban and Tiburon Island and (D) Ballenas Channel between the Baja
437 California Peninsula and Angel de la Guarda Island

Site Marker	M_2 tidal constituent	S_2 Tidal constituent	M_2 plus S_2 Tidal constituent
A	90 - 100 MW	$15 - 20$ MW	140 -150 MW
B	$60 - 70$ MW	$8 - 10$ MW	120 - 130 MW
C	$120 - 130$ MW	$10 - 15$ MW	$140 - 160$ MW
D	$60 - 70$ MW	$10 - 12$ MW	$120 - 130$ MW

438

439 ## 5. Discussion

440 In this paper, we have conducted two different sensitivity tests, as follows: (1) using three different bathymetry
441 products that were a combination of open source data and bespoke surveys; and (2) including different numbers
442 and combinations of tidal constituents, when predicting tidal levels and quantifying the tidal energy resource. In
443 the bathymetry sensitivity test, we compared three different bathymetry products which resulted in either an over
444 or under-estimation of the resource. We utilized exactly the same mesh resolution within the three simulations.
445 Thus, the computational mesh resolved the resource equally as well as the current speeds. Therefore, we assumed
446 that the changes of the resource are related to the bathymetry data which allow the water to be squeezed through
447 a smaller channel. Furthermore, the distribution of the water within the domain area especially in the narrow
448 channels within the midriff region would be different.

449 We considered four locations where current speeds are highest. At markers A, B and D (in Figure 5a) the annual
450 mean power as underestimated by more than a half, whereas at location C the annual mean power was
451 overestimated when using GEBCO_2014 only in comparison with GEBCO_2014 bathymetry merged with
452 CICESE. We find therefore that global and freely available bathymetry data products under-resolve the resource
453 by 75 %. For the location with fastest current speeds at San Lorenzo Passage, the annual mean power was
454 estimated to be around 50 MW when using freely available bathymetry data (GEBCO and ETOPO), while the
455 annual mean power increased to ~200 MW when using a bespoke dataset that was a combination of GEBCO and
456 higher resolution bathymetry provided by CICESE.

457 Uncertainty in tidal-stream resource estimation has been the focus for other geographic regions for good reason.
458 For example, two studies of the Johnstone Strait (British Columbia, Canada) found the annual mean tidal-stream
459 resource varied between 4015 MW [24] and 1320 MW [25] when using different bathymetry products. The main
460 differences in the estimated energy resource within this region could be a result of the use of different bathymetry
461 products, however, part of the differences could also be as a result of using differing methodologies to assess the
462 site. A study carried out by [26] concluded the flow constrains as a result of the bathymetry data, where the
463 coefficient of variation in the Florida Current is approximately 0.3%, resulted in a slight flow reduction. Similarly,
464 a study by [27] stated that the bathymetry data would alter the local tidal currents along Ireland's coastline;
465 consequently, the tidal current resource could vary significantly. Another study refers to the variability of the

466 power as a result of the velocity changes due to the bathymetry data [28]. They state that a combination of seabed
467 bathymetries and coastal shapes within the near-shore site in the Iroise Sea on the western Brittany coast, France
468 can alter the hydrodynamics and consequently the power density estimated can change.

469 In regard to tidal constituents, we compared the energy resource estimated using tidal levels predicted from 29
470 tidal constituents with time-series predicting just included the M_2 and S_2 tidal constitutes. The annual mean KPD
471 decreased by almost 1/3rd in San Lorenzo Passage, when just considering the M_2 plus S_2 constituents, suggesting
472 that diurnal and higher order harmonic constituents are important for accurate resource assessments in this region.
473 In the sensitivity tests, in which we compared the estimated energy estimates using all the constituents and just
474 M_2 plus S_2, the annual mean KPD had relatively large differences. The resource decreased by almost 1/3rd in San
475 Lorenzo Passage when using only the M_2 tidal constituents. Similarly, within the region of Ballenas channel the
476 annual mean power reduced significantly from 140 MW, when using all 29 tidal constituents, to 70 MW when
477 using only the M_2 tidal constituent. The variability of the resource using a limited number of tidal constituents to
478 predict the tidal current annually indicates that the M_2 constituent, as expected, plays an important role in the
479 energy calculation and contributes more than 50 % of the total energy resource, while S_2 contributes less (~20 %).
480 Therefore, the results suggested that diurnal and higher order harmonic constituents are important for accurate
481 resource assessments in this region.

482 A clear example of the variability of the energy resource when only M_2 and S_2 tidal constituents where used is
483 highlighted in a study by [29]. The theoretical undisturbed kinetic power density was estimated to be around 9
484 kW/m² at Casquets which is located in the Channel Islands (West of Alderney) when using just M_2 plus S_2 tidal
485 constituents. While an assessment carried out by [19] estimated the kinetic power density (in the same region and
486 utilizing the same methodology) of 7 kW/m² when using only the M_2 tidal constituent. Therefore, these results
487 pointed out that the kinetic power density was underestimated by 20 % when using only the M_2 tidal constituents.
488 Annual power variability using multiple tidal constituents was also assessed by Adcock et al. [30 and 31] where
489 the annual mean power was calculated in Pentland Firth, UK. The first paper (in 2013) estimated a mean power
490 of 1.9 GW when using M_2 plus S_2 tidal constituent, whereas a subsequent study conducted by the same authors
491 (in 2014) included eight main tidal constituents (K_1, K_2, M_2, MU_2, N_2, NU_2, O_1 and S_2). The results by [31]
492 indicated that the maximum available mean power is 2.16 GW while using only M_2 and M_2 plus S_2 tidal
493 constituents, the annual power reduces by approximately 20 % (1.74 GW) and 5% (2.15 GW), respectively.

494

6. Conclusions

496 To quantify the tidal-stream energy resource in any given region requires accurate bathymetry and hydrodynamic
497 processes. These need to be quantified and best practices identified. The best model validation against tide gauge
498 and ADCP measurements was obtained using the bespoke merged GEBCO and CICESE bathymetric dataset.
499 Model simulations using the merged bathymetry data predicted peak current speeds of up to 2.4 m/s in San
500 Lorenzo Passage whereas the maximum current speed using ETOPO alone was less than 1 m/s in San Lorenzo
501 Passage. In comparison, using bathymetry, model simulations predicted 1 m/s in the Ballenas channel and the
502 maximum current speed increased to 1.8 m/s, when using just ETOPO. We concluded that the tidal-stream
503 resource of the Gulf of California was higher when using higher-resolution bathymetry products, which has
504 interesting applications for the potential global resource and tidal energy industry. The number and combination

505   of tidal constituents used, also affected the annual energy estimations. In San Lorenzo passage. the annual mean

506   power varied from 15-20 MW, 90-100 MW and 140-150 MW, when using just the M_2 constituent, just S_2 and M_2

507   plus S_2, respectively. When using all 29 tidal constituents the annual mean power was estimated to be ~200 MW.

508   In conclusion, the results from this study indicate that it would be advisable to validate different bathymetry

509   products in order to ascertain accurate velocities at any given region. This validation should include the main

510   semi-diurnal and diurnal constituents to define the specific tidal-stream energy resource at any given site.

511

Acknowledgements

518

References

[1] Bahaj, A. S., & Myers, L. (2004). Analytical estimates of the energy yield potential from the Alderney Race (Channel Islands) using marine current energy converters. Renewable Energy, 29(12), 1931-1945. doi:http://dx.doi.org/10.1016/j.renene.2004.02.013

[2] Bahaj, A. S. (2011). Generating electricity from the oceans. Renewable and Sustainable Energy Reviews, 15(7), 3399-3416. doi:https://doi.org/10.1016/j.rser.2011.04.032.

[3] Neill, S. P., Angeloudis, A., Robins, P. E., Walkington, I., Ward, S. L., Masters, I., . . . Falconer, R. (2018). Tidal range energy resource and optimization – Past perspectives and future challenges. Renewable Energy, 127, 763-778. doi:https://doi.org/10.1016/j.renene.2018.05.007.

[4] Myers, L., & Bahaj, A. S. (2005). Simulated electrical power potential harnessed by marine current turbine arrays in the Alderney Race. Renewable Energy, 30(11), 1713-1731. doi:http://dx.doi.org/10.1016/j.renene.2005.02.008.

[5] Sutherland, G., Foreman, M., & Garrett, C. (2007). Tidal current energy assessment for Johnstone Strait, Vancouver Island. Proceedings of the Institution of Mechanical Engineers, Part A: Journal of Power and Energy, 221(2), 147-157. doi:10.1243/09576509jpe338

[6] Blanchfield, J., Garrett, C., Rowe, A., & Wild, P. (2008). Tidal Stream power resource assessment for Masset Sound, Haida Gwaii. Proceedings of the Institution of Mechanical Engineers, Part A: Journal of Power and Energy, 222(5), 485-492. doi:10.1243/09576509jpe585

[7] Draper, S., Adcock, T. A. A., Borthwick, A. G. L., & Houlsby, G. T. (2014). Estimate of the tidal stream power resource of the Pentland Firth. Renewable Energy, 63, 650-657. doi:https://doi.org/10.1016/j.renene.2013.10.015

[8] Mejia-Olivares, C. J., Haigh, I. D., Wells, N. C., Coles, D. S., Lewis, M. J., & Neill, S. P. (2018). Tidal-stream energy resource characterization for the Gulf of California, México. Energy, 156, 481-491. doi:https://doi.org/10.1016/j.energy.2018.04.074

[9] Badan-Dangon, A., Lavin, M. F., and Hendershott, M. C. (1991), Underway Doppler current profiles in the Gulf of California, *Eos Trans. AGU*, 72(19), 209– 218, doi:10.1029/EO072i019p00209-01.

[10] López, M., Candela, J., & García, J. (2008). Two overflows in the Northern Gulf of California. Journal of Geophysical Research: Oceans, 113(C8), n/a-n/a. doi:10.1029/2007JC004575

[11] Myers LE. Internal Report, Department of Civil and Environmental Engineering, University of Southampton, 2003.

[12] Iyer, A. S., Couch, S. J., Harrison, G. P., & Wallace, A. R. (2013). Variability and phasing of tidal current energy around the United Kingdom. Renewable Energy, 51(Supplement C), 343-357. doi:https://doi.org/10.1016/j.renene.2012.09.017

[13] Lewis, M., Neill, S. P., Robins, P. E., & Hashemi, M. R. (2015). Resource assessment for future generations of tidal-stream energy arrays. Energy, 83, 403-415. doi:http://dx.doi.org/10.1016/j.energy.2015.02.038

[14] Kapoor, D.C., (1981). General bathymetric chart of the oceans (GEBCO). Marine Geodesy, 5(1), pp.73–80.

[15] NOAA (2017). ETOPO1 Global Relief Model [online] United States of America. Available from https://www.ngdc.noaa.gov/mgg/global/. [Accessed March 2017].

[16] Jean-Michel Hervouet, "Hydrodynamics of Free Surface Flows: Modelling with the Finite Element Method", Wiley Blackwell, April 2007, 360p, ISBN-13: 978-0470035580.

[17] Blunden, L. S., & Bahaj, A. S. (2006). Initial evaluation of tidal stream energy resources at Portland Bill, UK. Renewable Energy, 31(2), 121-132. doi:http://dx.doi.org/10.1016/j.renene.2005.08.016

[18] Cornett, A., Durand, N., & Serrer, M. (2010). 3-D Modelling and Assessment of Tidal Current Resources in the Bay of Fundy, Canada.

[19] Coles, D. S., Blunden, L. S., & Bahaj, A. S. (2017). Assessment of the energy extraction potential at tidal sites around the Channel Islands. Energy, 124(Supplement C), 171-186. doi:https://doi.org/10.1016/j.energy.2017.02.023

566 [20] Pawlowicz, R., Beardsley, B., & Lentz, S. (2002). Classical tidal harmonic analysis including error estimates
567   in MATLAB using T_TIDE. Computers & Geosciences, 28(8), 929-937.
568   doi:https://doi.org/10.1016/S0098-3004(02)00013-4

569 [21] Lang, P., 2010. *TELEMAC modelling system User Manual*, EDF- R&D.

570 [22] Egbert, G. D., Bennett, A. F., & Foreman, M. G. G. (1994). TOPEX/POSEIDON tides estimated using a
571   global inverse model. Journal of Geophysical Research: Oceans, 99(C12), 24821-24852.
572   doi:10.1029/94JC01894

573 [23] Egbert, G. D., & Erofeeva, S. Y. (2002). Efficient Inverse Modeling of Barotropic Ocean Tides. Journal of
574   Atmospheric and Oceanic Technology, 19(2), 183-204. doi:10.1175/1520-
575   0426(2002)019<0183:eimobo>2.0.co;2

576 [24] Tarbotton, M., & Larson, M. (2006). Canada ocean energy atlas (phase 1) potential tidal current energy
577   resources analysis background. Report to Canadian Hydraulics Centre.

578 [25] Sutherland, G., Foreman, M., & Garrett, C. (2007). Tidal current energy assessment for Johnstone Strait,
579   Vancouver Island. Proceedings of the Institution of Mechanical Engineers, Part A: Journal of Power and
580   Energy, 221(2), 147-157. doi:10.1243/09576509jpe338

581 [26] Georgia Tech Research Corporation, (2011). Assessment of Energy Production Potential from Tidal Streams
582   in the United States. Final Project Report June 29, 2011. Award Number: DE-FG36-08GO18174.

583 [27] O'Rourke, F., Boyle, F., & Reynolds, A. (2014). Ireland's tidal energy resource; An assessment of a site in
584   the Bulls Mouth and the Shannon Estuary using measured data. Energy Conversion and Management, 87,
585   726-734. doi:http://dx.doi.org/10.1016/j.enconman.2014.06.089

586 [28] Thiébaut, M., & Sentchev, A. (2015). Estimation of Tidal Stream Potential in the Iroise Sea from Velocity
587   Observations by High Frequency Radars. Energy Procedia, 76, 17-26.
588   doi:http://dx.doi.org/10.1016/j.egypro.2015.07.835

589 [29] Guillou, N., Neill, S. P., & Robins, P. E. (2018). Characterising the tidal stream power resource around France
590   using a high-resolution harmonic daase. Renewable Energy, 123, 706-718.
591   doi:https://doi.org/10.1016/j.renene.2017.12.033

592 [30] Adcock, T. A. A., Draper, S., Houlsby, G. T., Borthwick, A. G. L., & Serhadlıoğlu, S. (2013). The available
593   power from tidal stream turbines in the Pentland Firth. Proceedings of the Royal Society A: Mathematical,
594   Physical and Engineering Science, 469(2157). doi:10.1098/rspa.2013.0072

595 [31] Adcock, T. A., Draper, S., Houlsby, G. T., Borthwick, A. G., & Serhadlıoğlu, S. (2014). Tidal stream power
596   in the Pentland Firth – long-term variability, multiple constituents and capacity factor. Proceedings of
597   the Institution of Mechanical Engineers, Part A: Journal of Power and Energy, 228(8), 854-861.
598   doi:10.1177/0957650914544347

599 [32] Hagerman, G., Polagye, B., Bedard, R., & Previsic, M. (2006). Methodology for estimating tidal current
600   energy resources and power production by tidal in-stream energy conversion (TISEC) devices.

601 [33] Cornett A. (2006), Inventory of Canada's Marine renewable energy resources. Canadian Hydraulics centre.
602   CHC-TR-041. April 2006.

603 [34] O'Rourke, F., Boyle, F., & Reynolds, A. (2010). Tidal current energy resource assessment in Ireland: Current
604   status and future update. Renewable and Sustainable Energy Reviews, 14(9), 3206-3212.
605   doi:http://dx.doi.org/10.1016/j.rser.2010.07.039

606 [35] Georgia Tech Research Corporation, (2011). Assessment of Energy Production Potential from Tidal Streams
607   in the United States. Final Project Report June 29, 2011. Award Number: DE-FG36-08GO18174.

608 [36] Karsten, R., Swan, A., & Culina, J. (2013). Assessment of arrays of in-stream tidal turbines in the Bay of
609   Fundy. Philosophical Transactions of the Royal Society A: Mathematical,
610   Physical and Engineering Sciences, 371(1985). doi:10.1098/rsta.2012.0189

611 [37] Georgia Tech Research Corporation, (2013). Assessment of Energy Production Potential from Ocean
612   Currents along the United States Coastline. Final Project Report September 15, 2013. Award Number:
613   DE-EE0002661. (MFanually edited).

614

615   [38] Serhadlıoğlu, S., Adcock, T. A. A., Houlsby, G. T., Draper, S., & Borthwick, A. G. L. (2013). Tidal stream
616   energy resource assessment of the Anglesey Skerries. International Journal of Marine Energy, 3–4, e98-
617   e111. doi:https://doi.org/10.1016/j.ijome.2013.11.014

618   [39] Work, P. A., Haas, K. A., Defne, Z., & Gay, T. (2013). Tidal stream energy site assessment via three-
619   dimensional model and measurements. Applied Energy, 102(Supplement C), 510-519.
620   doi:https://doi.org/10.1016/j.apenergy.2012.08.040

621   [40] Blunden, L. S., Bahaj, A. S., & Aziz, N. S. (2013). Tidal current power for Indonesia? An initial resource
622   estimation for the Alas Strait. Renewable Energy, 49, 137-142.
623   doi:https://doi.org/10.1016/j.renene.2012.01.046

624   [41] Plew, D. R., & Stevens, C. L. (2013). Numerical modelling of the effect of turbines on currents in a tidal
625   channel – Tory Channel, New Zealand. Renewable Energy, 57, 269-282.
626   doi:http://dx.doi.org/10.1016/j.renene.2013.02.001

627   [42] Wang, T., & Yang, Z. (2017). A modelling study of tidal energy extraction and the associated impact on tidal
628   circulation in a multi-inlet bay system of Puget Sound. Renewable Energy.
629   doi:http://dx.doi.org/10.1016/j.renene.2017.03.049

630   [43] Tang, H. S., Qu, K., Chen, G. Q., Kraatz, S., Aboobaker, N., & Jiang, C. B. (2014). Potential sites for tidal
631   power generation: A thorough search at coast of New Jersey, USA. Renewable and Sustainable Energy
632   Reviews, 39, 412-425. doi:https://doi.org/10.1016/j.rser.2014.07.051

633   [44] Osorio, A. F., Ortega, S., & Arango-Aramburo, S. (2016). Assessment of the marine power potential in
634   Colombia. Renewable and Sustainable Energy Reviews, 53, 966-977.
635   doi:http://dx.doi.org/10.1016/j.rser.2015.09.057

636   [45] González-Gorbeña, E., Rosman, P. C. C., & Qassim, R. Y. (2015). Assessment of the tidal current energy
637   resource in São Marcos Bay, Brazil. Journal of Ocean Engineering and Marine Energy, 1(4), 421-433.
638   doi:10.1007/s40722-015-0031-5

639   [46] Orhan, K., Mayerle, R., & Pandoe, W. W. (2015). Assesment of Energy Production Potential from Tidal
640   Stream Currents in Indonesia. Energy Procedia, 76, 7-16.
641   doi:http://dx.doi.org/10.1016/j.egypro.2015.07.834

642   [47] Goward Brown, A. J., Neill, S. P., & Lewis, M. J. (2017). Tidal energy extraction in three-dimensional ocean
643   models. Renewable Energy. doi:http://dx.doi.org/10.1016/j.renene.2017.04.032

644   [48] Alonso, R., Jackson, M., Santoro, P., Fossati, M., Solari, S., & Teixeira, L. (2017). Wave and tidal energy
645   resource assessment in Uruguayan shelf seas. Renewable Energy.
646   doi:http://dx.doi.org/10.1016/j.renene.2017.03.074.

647   [49] Marta-Almeida, M., Cirano, M., Guedes Soares, C., & Lessa, G. C. (2017). A numerical tidal stream energy
648   assessment study for Baía de Todos os Santos, Brazil. Renewable Energy, 107, 271-287.
649   doi:https://doi.org/10.1016/j.renene.2017.01.047

650   [50] Thiébaut, M., & Sentchev, A. (2017). Asymmetry of tidal currents off the W.Brittany coast and assessment
651   of tidal energy resource around the Ushant Island. Renewable Energy, 105, 735-747.
652   doi:http://dx.doi.org/10.1016/j.renene.2016.12.082

653   [51] Campbell, R., Martinez, A., Letetrel, C., & Rio, A. (2017). Methodology for estimating the French tidal
654   current energy resource. International Journal of Marine Energy, 19(Supplement C), 256-271.
655   doi:https://doi.org/10.1016/j.ijome.2017.07.011

656

657

Appendix A Table 1 List of studies that mentioned and used one or more different
Bathymetry products at the time of writing.

Location	Current speed	Modelling approach	Bathymetry used	Reference
USA, East and west coast.	From 1.5 up to 6.67 m/s	WXTide32	National Oceanic and Atmospheric Administration NOAA, USA	[32]
Canada, East and west coast.	average flow speed of 2.11 m/s	WebTide Tidal Prediction Model (v0.7.1)	Canadian Hydrographic Service, admiralty charts by Nautical Data International (NDI).	[33]
Canada Northwest Territories British Columbia Quebec Nunavut New Brunswick PEI Nova Scotia Newfoundland	From 2.7 m/s to 8.23 m/s. Please see reference for full details	Tide 2D	Nautical data including Canadian Sailing Directions and a total of 950 nautical charts by The Canadian Hydrographic Service	[24]
UK, Portland Bill	3.6 m/s	TELEMAC 2D	Southampton Oceanography Centre bathymetry survey	[17]
Canada, Johnstone Strait	4.7 to 7.7 m/s	TIDE2D	Canadian Hydrographic Service and the National Oceanic and Atmospheric Administration NOAA, USA.	[25]
Masset Sound, located in Haida Gwaii	2.5 m/s	One-dimensional model	Bathymetry data provided by Canadian Hydrographic Service department of fishery and oceans	[6]
Bay of Fundy, Canada	Average spring tide excess 5 m/s	TELEMAC 3D	High-resolution bathymetric by Natural Resources Canada using a multi-beam sonar. Bathymetric contours by the Canadian hydrographic service and various data sets collected by Massachusetts Geographic Information System.	[18]
Ireland	Above 1.9 m/s	MIKE 21	local bathymetry provided by the Danish Hydrographic Institute	[34]
Georgia Coast, USA	Mean from 0.34 to 1.07 m/s	ROMS	The medium resolution shoreline (1/70,000) data from National. Oceanic and Atmospheric Administration (NOAA) and the digital sounding data from National Geophysical Data Centre (NGDC)	[41]
USA coastline	1 m/s	ROMS	Hydrographic Surveys Database (NOS, 2008a). NOAA Electronic Navigational Charts (NOAA, 2008a) and National Geophysical Data Centre Geophysical Data System database (GEODAS) (NGDC).	[35]
Canada, Bay of Fundy	More than 5 m/s	FVCOM	Survey by Bedford Institute of Oceanography and the bathymetry used by Tarbotton and Larson (2006). Triton consultants	[36]
Coastline, USA		HYCOM, ROMS, HYCOM GLOBAL, NCOM	National Oceanic and Atmospheric Administration NOAA, USA	[37]

Location	Current speed	Modelling approach	Bathymetry used	Reference
UK, Pentland Firth	5 m/s	ADCIRC	The bathymetry data were purchased from Seazone. http://www.seazone.com/	[30]
UK, Anglesey Skerries	Up to 1.4 m/s	ADCIRC	Bathymetry data provided by Seazone. http://www.seazone.com/	[38]
South Carolina, USA	0.87 m/s	ROMS 3D	US National Ocean Service data and boat surveys	[39]
Indonesia, Alas strait	1.2 m/s	The Princeton Ocean Model (POM)	Bathymetric chart of Alas Strait (map Number 293, edition 2006) provided by Indonesian Navy Hydro-Oceanographic Division.	[40]
New Zealand, Tory Channel	2 m/s	RICOM	Swath bathymetry and digitizing of contours and soundings from the Land Information New Zealand Hydrographic Charts (NZ 463, 4633, 614e615, 6142, 6151e6154, 6212).	[41]
Puget Sound, Canada	2 m/s during spring tide	FVCOM	Bathy from digital elevation model and light detection and ranging (LiDAR).	[42]
Pentland Firth, UK	3 m/s	ADCIRC	The bathymetry data was the same as Adcock et al. (2013). purchased from Seazone http://www.seazone.com/	[31]
Ireland, Bull mouth and Shannon Estuary.	2.02 m/s during spring tide	Measure data	No provided information	[27]
Coast of New jersey, USA (please see reference for details of the 21 points)	1.26 m/s	Finite Volume Coastal Ocean Model (FVCOM)	NOAA Coastal Services Centre and ETOP5.	[43]
Colombia, Buenaventura Bay.	Mean current speed 0.8 m/s	H2D	ETOPO1 and Sistema de Modelado costero (SMC) bathymetry module from University of Cantabria Spain.	[44]
Brazil, Sao Marcos Bay.	2.63 m/s	SisBaHiA	Digitising nautical charts for São Marcos Bay	[45]
UK, Irish Sea	Above 2.5 m/s	ROMS	Digitised Admiralty data. (http://digimap.edina.ac. uk)	[13]
Indonesia, Strait of Larantuka	3 to 4 m/s	Delft3D	GEBCO 30 arc-second	[46]
Pentland, Firth UK	2 m/s	ROMS	GEBCO 30 arc-second	[47]
Puget Sound, Canada	2 m/s during spring tide	FVCOM	Bathy from digital elevation model and light detection and ranging (LiDAR).	[42]
Uruguay	0.35 m/s	MOHID - Water Modelling System	GEBCO 30 arc-second and regional bathymetry charts.	[48]
Brazil, Baía de Todos os Santos	Max 1.0 m/s	ROMS	No provided information	[49]
France, W. Brittany coast.	From 1 m/s to 4 m/s	Data Analysis	No provided information	[50]
Channel Islands, UK and France.	>2.5 m/s mean spring tide	TELEMAC 2D	T-Carta 90 + GEBCO	[19]
France, English Channel.	1.5 m/s average	MARS2D	Bathymetry provided by SHOM-IFREMER	[60]

661

662

663

664

665

666   **Appendix B TELEMAC Steering file**

667

668   Example of the steering file used in the model simulation within the Gulf of California created in

669   TELEMAC 2D. A brief explanation of the purpose of the variables is provided, in brackets, for each line.

670

671   /   INFORMATION ENVIRONMENT   /

672   /---/

673   BOUNDARY CONDITIONS FILE   = 'BC_BATHY_CICESE.cli' (*Formatted boundary*

674   *conditions file*)

675   GEOMETRY FILE   = 'Selafin_BCF_with_Bathy_CICESE.slf' (*Binary mesh file*

676   *containing mesh coordinates*)

677   BINARY DATABASE 1 FOR TIDE   = './tpxo/h_tpxo7.2' (*forcing file elevation*)

678   BINARY DATABASE 2 FOR TIDE   = './tpxo/u_tpxo7.2' (*forcing file tidal velocities*)

679   MINOR CONSTITUENTS INFERENCE   = YES (*For TPXO tidal data base only. Inference of minor*

680   *constituents from the one read in input files linked to keywords BINARY DATABASE 1 FOR TIDE and BINARY DATABASE*

681   *2 FOR TIDE.*)

682   RESULTS FILE   = 'Results_33days_BCF_CICESE.slf' (*Binary results file*)

683   /---/

684   /   GENERAL OPTIONS

685   /---/

686   VARIABLES FOR GRAPHIC PRINTOUTS   = U,V,S,H,B (*U,V=Flow speeds, H=Depth, S =Free*
687   *surface, B= Bottom friction*)
688   TIME STEP   = 10 (*Seconds*)

689   NUMBER OF TIME STEPS   = 285120 / 33 days every 10 seconds (*Total*

690   *duration of simulation*)

691   NUMBER OF FIRST TIME STEP FOR GRAPHIC PRINTOUTS = 1 (*Period between output to*

692   *results file (time steps)*)

693   GRAPHIC PRINTOUT PERIOD   = 60 (*Period between output to results file (time steps)*)

694   LISTING PRINTOUT PERIOD   = 10 (*Period between listing file output (time steps*)

695   MASS-BALANCE   = YES (*Determines whether or not the mass-balance over*

696   *the entire domain is checked. For each time step*)

697   /---/

698   /   INITIAL CONDITIONS

699   /---/

700   ORIGINAL DATE OF TIME   = 2015;11;28 (*initial simulation date*)

701   ORIGINAL HOUR OF TIME   = 0;0;0 (*Initial simulation time*)

702   INITIAL CONDITIONS   = 'TPXO SATELLITE ALTIMETRY' (*This is used to*

703   *define initial water depth conditions.*)

704   /--/

705   /   BOUNDARY CONDITIONS

706   /--/

707   OPTION FOR LIQUID BOUNDARIES   = 2;2 (*Thompson method to find unknown boundary*
708   *velocities*)

709   /   TIDE CONDITIONS   /

710   /--/

711   OPTION FOR TIDAL BOUNDARY CONDITIONS   = 1 (*Option for tidal boundary conditions.*

712   *For real tides, option 1 is recommended.*)

713   TIDAL DATA BASE   = 2 (*Number 2 corresponds to TPXO forcing*

714   *file*)

715   SPHERICAL COORDINATES   = YES (*Spherical Mercator coordinates*
716   *for simulations*
717   */over large domains*)

718   LATITUDE OF ORIGIN POINT   = 23.107399 (*Used to determine tide-*

719   *generating potential*)

720   LONGITUDE OF ORIGIN POINT   = -111.902617 (*For spherical*
721   *coordinates*)
722

723   SPATIAL PROJECTION TYPE   = 2

724   GEOGRAPHIC SYSTEM   = 5 (*Mercator for TELEMAC*)
725
726   CORIOLIS   = YES (*Includes the effect of the Coriolis*

727   *force*)

728   /--/

729   /   HYDRODYNAMICS-PHYSICAL SETUP

730   /--/

731   LAW OF BOTTOM FRICTION   = 4 (*Number 4 correspond to manning law that was used to*
732   *model bed friction over the whole domain*)
733   FRICTION COEFFICIENT   = 0.030 (*Friction coefficient relating to Manning law friction*
734   *applied uniformly over the domain*)
735   TURBULENCE MODEL   = 4 (*Constant turbulent viscosity throughout the*
736   */domain, Smagorinski model.*)

737   DIFFUSION OF VELOCITY   = YES

738   VELOCITY DIFFUSIVITY   = 1.E-6 (*for option 4, the keyword VELOCITY DIFFUSIVITY must*

739   *be the value of molecular viscosity (10-6 m2/s) because it is used as such in the turbulence model.*)

```
740    /-----------------------------------------------
741    /          ADVECTION-DIFFUSION
742    /-----------------------------------------------
743    TYPE OF ADVECTION                         = 1;5 (these numbers specifying the variables and method
744    are used to solve the advection step, the first number indicates the variable U and V (velocity components and the number 5
745    indicated the method that is PSI distributive scheme, mass-conservative (mandatory for H),
746
747    SUPG OPTION                                = 0;0 (Upwind scheme, no upwinding)
748    MATRIX STORAGE                             = 3 (keyword configures the type of matrix
749    storage. It is strongly recommended to use the default value as 3)
750    FREE SURFACE GRADIENT COMPATIBILITY       = 0.6
751    TREATMENT OF THE LINEAR SYSTEM            = 2 (Uses velocity from momentum
752    equation rather than continuity equation to improve computational efficiency)
753    TREATMENT OF FLUXES AT THE BOUNDARIES     = 1;1
754    INFORMATION ABOUT SOLVER                  = YES
755    MAXIMUM NUMBER OF ITERATIONS FOR SOLVER   = 100
756    SOLVER                                     = 3 (Conjugate gradient method for the
757    /hydrodynamic propagation step)
758    SOLVER ACCURACY                           = 1.E-6 (Accuracy during propagation
759    step)
760    /-----------------------------------------------------------------/
761    /               NUMERICAL OPTIONS
762    /-----------------------------------------------------------------/
763    ZERO                                       = 1.E-10
764    TIDAL FLATS                                = YES (Enables wetting and drying in
765    shallow regions)
766    OPTION FOR THE TREATMENT OF TIDAL FLATS   = 1 (Enables wetting and drying in shallow
767    regions)
768    TREATMENT OF NEGATIVE DEPTHS              = 2 (specifies the type of treatment of the
769    negative depths, there are three options: 0 : no treatment, 1 : smoothing of negative depth,  2 : Flux control).
770    CONTINUITY CORRECTION                      = YES (corrects velocity particularly in
771    the boundary points)
772    DISCRETIZATIONS IN SPACE                   =  11;11  (binary  triangle  (4  node
773    triangle) velocity and linear depth)
774    /-----------------------------------------------
775    /   PROPAGATION                     /
776    /-----------------------------------------------
```

777   IMPLICITATION FOR DEPTH   = 1. (*To account for semi-implicit discretization of*

778   *time*)

779   IMPLICITATION FOR VELOCITY   = 1. (*To account for semi-implicit discretization of*

780   *time*)

781   IMPLICITATION FOR DIFFUSION OF VELOCITY   = 1.(*Recommend as default where the wave*

782   *equation is not applied)*

783   MASS-LUMPING ON H   = 1. (*This number refers to the method to*

784   *accelerate the computational simulation as well as consider the setting values of H within the model)*

785   &FIN (*end of the steering file)*

786